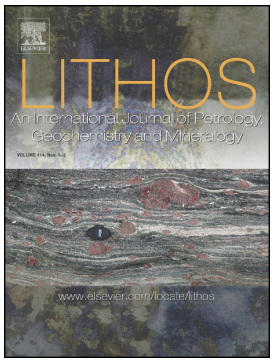

The recycling of chromitites in ophiolites from southwestern North America

José M. González-Jiménez, Antoni Camprubí, Vanessa Colás, William L. Griffin, Joaquín A. Proenza, Suzanne Y. O'Reilly, Elena Centeno-García, Antonio García-Casco, Elena Belousova, Cristina Talavera, Júlia Farré-de-Pablo, Takako Satsukawa

PII: S0024-4937(17)30332-8
DOI: doi:10.1016/j.lithos.2017.09.020
Reference: LITHOS 4426

To appear in:

Received date: 25 July 2017
Accepted date: 20 September 2017

Please cite this article as: José M. González-Jiménez, Antoni Camprubí, Vanessa Colás, William L. Griffin, Joaquín A. Proenza, Suzanne Y. O'Reilly, Elena Centeno-García, Antonio García-Casco, Elena Belousova, Cristina Talavera, Júlia Farré-de-Pablo, Takako Satsukawa , The recycling of chromitites in ophiolites from southwestern North America. The address for the corresponding author was captured as affiliation for all authors. Please check if appropriate. Lithos(2017), doi:10.1016/j.lithos.2017.09.020

The recycling of chromitites in ophiolites from southwestern North America

José M. González-Jiménez[a,b], Antoni Camprubí[c], Vanessa Colás[c,b], William L. Griffin[b], Joaquín A. Proenza[d], Suzanne Y. O'Reilly[b], Elena Centeno-García[c], Antonio García-Casco[a,e], Elena Belousova[b], Cristina Talavera[f], Júlia Farré-de-Pablo[d], Takako Satsukawa[b,g]

a. Departamento de Mineralogía y Petrología, Facultad de Ciencias, Universidad de Granada, Avda. Fuentenueva s/n, 18002 Granada, Spain.
b. ARC Centre of Excellence for Core to Crust Fluid Systems (CCFS), and GEMOC National Key Centre, Macquarie University, Sydney, NSW 2109, Australia.
c. Instituto de Geología, Universidad Nacional Autónoma de México, Ciudad Universitaria, 04510 Ciudad de México, Mexico.
d. Departament de Mineralogia, Petrologia i Geologia Aplicada, Universitat de Barcelona (UB), 08028 Barcelona, Spain.
e. Instituto Andaluz de Ciencias de la Tierra (IACT), CSIC-UGR, Avda. de las Palmeras 4, 18100 Armilla, Granada, Spain
f. John de Laeter Centre, Faculty of Science and Engineering, Curtin University, Perth, WA 6102, Australia.
g. Department of Geophysics, Kyoto University, Kyoto, 606-8502, Japan.

Submitted

to

Lithos

*Corresponding author: José María González Jiménez
Address: Departamento de Mineralogía y Petrología, Facultad de Ciencias, Universidad de Granada, Granada, Spain
Avda. Fuentenueva s/n 18002 Granada
Phone: +34 958 248 535
E-mail: jmgonzj@ugr.es

Abstract

Podiform chromitites occur in mantle peridotites of the Late Triassic Puerto Nuevo Ophiolite, Baja California Sur State, Mexico. These are high-Cr chromitites [Cr# (Cr/Cr+Al atomic ratio = 0.61-0.69] that contain a range of minor- and trace-elements and show whole-rock enrichment in IPGE (Os, Ir, Ru). These features are similar to those of high-Cr ophiolitic chromitites crystallised from melts similar to high-Mg island-arc tholeiites (IAT) and boninites in supra-subduction-zone mantle wedges. Crystallisation of these chromitites from S-undersaturated melts is consistent with the presence of abundant inclusions of platinum-group minerals (PGM) such as laurite (RuS_2)-erlichmanite (OsS_2), osmium and irarsite (IrAsS) in chromite, that yield $T_{MA} \approx T_{RD}$ model ages peaking at ~325 Ma. Thirty-three xenocrystic zircons recovered from mineral concentrates of these chromitites yield ages (2263 ± 44 Ma to 278 ± 4 Ma) and Hf-O compositions [$\varepsilon_{Hf}(t)$ = -18.7 to +9.1 and ^{18}O values <12.4‰] that broadly match those of zircons reported in nearby exposed crustal blocks of southwestern North America. We interpret these chromitite zircons as remnants of partly digested continental crust or continent-derived sediments on oceanic crust delivered into the mantle via subduction. They were captured by the parental melts of the chromitites when the latter formed in a supra-subduction zone mantle wedge polluted with crustal material. In addition, the Puerto Nuevo chromites have clinopyroxene lamellae with preferred crystallographic orientation, which we interpret as evidence that chromitites have experienced high-temperature and ultra high-pressure conditions (<12 GPa and ~1600 °C). We propose a tectonic scenario that involves the formation of chromitite in the supra-subduction zone mantle wedge underlying the Vizcaino intra-oceanic arc *ca* 250 Ma ago, deep-mantle recycling, and subsequent diapiric exhumation in the intra-oceanic basin (the San Hipólito marginal sea) generated during an extensional stage of the Vizcaino intra-oceanic arc *ca* 221 Ma ago. The T_{RD} ages at ~325 Ma record a partial melting event in the mantle prior to the construction of the Vizcaino intra-oceanic arc, which is probably related to the Permian continental subduction, dated at ~ 311 Ma.

Keywords: Chromitite, zircon, UHP conditions, mantle recycling, Baja California.

1. INTRODUCTION

Chromitites are rocks that consist mainly of (Cr, Al)-rich spinel and can be counted among the most enigmatic components of the Earth's mantle. Today, the application of advanced methods of mineral thermodynamics, geochemistry, isotope geology and geophysics, gives us a more accurate view of chromitite genesis and its implications for large-scale geodynamic processes. The most accepted hypothesis is that chromitites form as products of melt-rock reactions and subsequent mingling of basaltic melts in the shallower part of the upper mantle, above supra-subduction zones (González-Jiménez et al., 2011; Arai and Miura, 2016). However, the recent discovery of ultra-high pressure minerals (UHP ≥ 0.4 GPa; diamond, TiO_2 II, stishovite pseudomorphs) coexisting with others that were formed under super-reducing conditions (*v.g.*, native elements, alloys, carbides, nitrides; i.e., the SuR-UHP assemblage of Griffin et al., 2016) or in the continental crust (e.g., zircons, K-feldspar, plagioclase, kyanite, garnet or quartz; Robinson et al., 2015) has renewed the controversy on the actual origin of mantle-hosted chromitites. Diamonds indicate depths > 120 km, whereas coesite pseudomorphs after stishovite and clinopyroxene exsolution lamellae in some chromite grains indicate metamorphism at depths of > 300 km (Yang et al., 2007; Yamamoto et al., 2009; Zhang et al., 2017). Therefore, any petrogenetic model for mantle-derived chromitites must reconcile the presence of UHP minerals with abundant evidence for shallow formation. Nowadays the debate focuses on the (1) *plume model, (2) slab contamination* and (3) *subduction-recycling* model or their derivatives.

The *plume model* explains the mixture of crustal minerals and the mantle SuR-UHP assemblage as a result of the mechanical entrapment of all these minerals by chromite growing from Cr-rich melts during transport from the Mantle Transition Zone (MTZ) to the upper mantle (Ruskov et al., 2010; Xiong et al., 2015; Xu et al., 2015; Yang et al., 2015; Wu et al., 2016). In this model, a mantle plume rises from the lower mantle through the MTZ or directly from the MTZ, where it collects a mixture of crustal materials brought there through earlier subduction and super-reducing minerals from the transition zone itself. These are then carried though the upper mantle on the upwelling plume to be incorporated in the magma system beneath a spreading system. However, as stressed by Rollinson (2016), this model requires the

"happy coincidence of mantle plume and spreading centre, which is not often observed" [*sic*]. In addition, recent experiments conducted by Zhang et al. (2017) in the system pyrolite+chromite at 15 GPa and 1800°C have shown that Cr is preferentially partitioned into garnet, rather than melt. Thus, melts formed by the deep partial melting of pyrolite should be Cr-poor under both dry and hydrous conditions, and therefore neither chromite, nor its high-pressure and high-temperature polymorphs can be formed through direct crystallisation from melts at the top of the MTZ.

The *slab contamination* model proposed by Zhou et al. (2014) and Robinson et al. (2015) requires the tearing and breakoff of a subducted slab during subduction initiation, which creates a slab window through which the underlying asthenosphere rises and melts to generate Cr-rich mafic magmas. In this model, highly reduced and ultra-high-pressure minerals may have been brought by the uprising asthenosphere at mid-ocean ridges due to mantle convection. Zhou et al. (2014) suggested that chromite grains could be transported by the ascending melts against gravity, attached to water-rich pools segregated from the decompressing basaltic melt. However, while some suprasubduction zone basaltic melts may be rich in volatiles, the exsolution of volatile-rich bubbles could only occur at very low pressures in the shallow mantle (< 0.5 GPa; Matveev and Ballhaus, 2002). Therefore, it is unlikely that a dense mineral like chromite could be carried up against gravity by basaltic melts over hundreds of kilometres from the slab window to the shallow mantle. Moreover, Electron Backscatter Diffraction (EBSD) maps of chromites with exsolved diopside needles from UHP Tibetan high-Cr chromitites have shown that large chromite grains with plastic deformation enclose relict chromite subgrains (Satsukawa et al., 2015; Xiong et al., 2017), suggesting the overgrowth of coarse-grained chromite on pre-existing chromite during high-temperature, high-pressure metamorphism. These microstructures of the chromite are inconsistent with the rise of single chromite grains, or even small volume of chromitites.

The *subduction-recycling* model implies that chromitites initially crystallised in the upper mantle portion of oceanic or continental mantle wedges above a subducting slab, as products of melt-rock reaction and subsequent melt-melt mixing processes, were subducted to the Mantle Transition Zone where they became

metamorphosed at UHP conditions, and then were exhumed together with their host dunite/harzburgite at spreading centres as mantle diapirs (Arai, 2013; Miura et al., 2012; McGowan et al., 2015; Arai and Miura, 2016; Griffin et al., 2016). Thus, Arai (2013) has suggested that two types of chromitites can coexist in the ophiolites, depending on whether they underwent mantle recycling or not. Concordant UHP chromitites with silicate lamellae and minerals of the Sur-UHP assemblage, and late generations of discordant low-pressure chromitites lack these minerals. In this model, crustal minerals (e.g., zircons) were trapped in chromite during its growth at low pressures in the shallow mantle whereas UHP minerals are incorporated into chromite during metamorphism in the MTZ (Griffin et al., 2016). However, the latter interpretation has been developed after the observations in the Tibetan chromitites and peridotites, and has not been tested yet in other scenarios.

In order to contribute to the ongoing debate, we have examined chromitites of the Puerto Nuevo Ophiolite in the Baja California Sur state, Mexico. This is an example of a chromitite-bearing arc-basin ophiolite generated in the latest stage of evolution of an intra-oceanic arc (Kimbrough and Moore, 2003). This scenario gives us an opportunity to evaluate the genesis and evolution of chromitites within the framework of a previously unrecognised geotectonic setting: a passive continental margin that evolved into an arc-basin. We analysed whole-rock PGE contents and used *in situ* laser-ablation techniques to determine (1) the major-, minor, and trace-element composition of chromite, (2) the isotopic composition of Os in individual PGMs and U-Pb and Lu-Hf in zircons, and (3) micro-Raman to characterize the exsolved silicates in chromite. These data are integrated with recently published empirical and experimental data in order to better constrain the petrogenesis of the Puerto Nuevo chromitites in the geological context of the Cordilleran margin of Western North America.

2. GEOLOGICAL BACKGROUND

2.1. Ultramafic rocks in the Peninsula

The Peninsula is a mountainous region located on the western side of the Baja California Peninsula, approximately 600 km south of the westernmost Mexico-U.S.

border (Fig. 1). Geologically, the Peninsula, together with the Cedros and San Benito islands to the north, belongs to the Cochimi tectonostratigraphic composite terrane (Sedlock et al., 1993). Along the southwestern edge of the Peninsula, slices of mafic-utramafic rocks associated with volcanic and sedimentary rocks are discontinuously exposed in a northwest-trending belt from Punta Quebrada to Punta San Hipólito (Fig. 1).

The Puerto Nuevo sequence contains by far the best exposures of mafic-ultramafic rocks on the Peninsula. It crops out in a N70°W-trending belt that extends almost continuously for ~32 km from the north of the Sierra del Placer to the Sierra Morro Hermoso, as well as scattered smaller outcrops north of Punta Quebrada (Fig. 1). This sequence consists, from bottom to top, of three members separated by tectonic contacts: (1) ultramafic, (2) gabbroic and (3) extrusive complex (Castro-Leyva et al., 2001). In the literature, the Puerto Nuevo sequence is referred as the *shredded ophiolite*, the *Norte Terrane/ophiolite* or the *Puerto Nuevo Mélange/Ophiolite* (Castro-Leyva et al., 2001 and references therein).

Assemblages of mafic-ultramafic rocks associated with the volcanic rocks are also exposed further south and east of the Sierra de San Andrés, the Central part of the Sierra El Placer and along the south coast of the Peninsula from Punta San Pablo to Punta San Hipólito (Fig. 1). There, the sequence includes strongly serpentinised harzburgite with tectonite overlain by layered gabbros, which are topped by pillow basalts that include radiolarian cherts. Fossils of *Halobia* sp. and *Monotis* sp. have been reported in sediments intercalated with pillow basalts from Punta San Hipólito, Sierra de San Andrés and Punta Quebrada, which constrain the age of these extrusive rocks to the Carnian-Norian boundary (221 ± 9 Ma; Kimbrough and Moore, 2003). This sequence of rocks has been named the *Coherent Ophiolite*, *La Costa ophiolite*, the *Sierra de Placeres Mélange* and as part of the *Sur Terrane/Ophiolite* (Castro-Leyva et al., 2001 and references therein).

West of the Sierra del Placer, both the Puerto Nuevo Sequence and the La Costa Sequence are overthrust by the Late Triassic-Early Jurassic San Hipólito Formation (Castro-Leyva et al., 2001). This formation is made up of a sequence of volcanic and volcanoclastic rocks, with lesser amounts of fossiliferous carbonate rocks interpreted as the remnants of an intra-oceanic arc (Centeno-García, 2017). A Late Triassic paleontological age determined from radiolarians in the La Costa pillow

basalts and the San Hipólito Formation matches well that obtained for intruding plagiogranites in Puerto Nuevo; this coincidence has led to the suggestion that the two sequences are part of a single disrupted ophiolite complex (Kimbrough and Moore, 2003). In this model, the Puerto Nuevo and La Costa mafic-ultramafic rocks would correspond to remnants of the mantle-crust transition of an oceanic marginal basin that developed very close to a volcanic arc represented by the San Hipólito Formation (Kimbrough and Moore, 2003). Kimbrough and Moore (2003) introduced the term " Peninsula ophiolite" to refer collectively to both ophiolite remnants. In this second model, the two sequences mentioned above would correspond to ophiolites generated at different times and in different tectonic settings along the foreland of the Cordilleran margin of North America from Pre-Late Triassic to Liassic time.

2.2. The Puerto Nuevo Sequence

In the Peninsula, chromite deposits have only been reported from ultramafic rocks of the Puerto Nuevo sequence. Here we provide a brief summary of these rocks, based on the previous characterisations by Castro-Leyva et al. (2001), which divide the sequence into four main zones (Fig. 2): (1) Lower Serpentinite Breccia, (2) Peridotite Zone, (3) Critical Zone and (4) Gabbroic Zone.

The *Lower Serpentinite Breccia* is the lowermost known part of the Puerto Nuevo Sequence. It crops out near the village of Puerto Nuevo and in the Sal-Si-Puedes Canyon (Fig. 2). Following pre-existing interpretations, Castro-Leyva et al. (2001) have regarded this unit as a tectonic mélange, i.e., the Puerto Nuevo Mélange. The boundary between the serpentinite breccia and the overlying serpentinised harzburgite is unclear in the field. As noted above, this Lower Serpentinite Breccia contains isolated blocks of pyroxenite and amphibolite, identical to those reported in San Pablo Metamorphic Complex further south of Puerto Nuevo.

The *Peridotite Zone* consists, from bottom to top, of variably (85-100%) serpentinised harzburgite, dunite hosting chromitite bodies, and lesser amounts of wehrlite and pyroxenite. Most of the sequence consists of harzburgite made up of olivine replaced by lizardite, and lesser amounts pyroxene transformed to bastite (Castro-Leyva et al., 2001). The dunites consist chiefly of olivine replaced by lizardite and chrysotile, with accessory chromite (< 5% modal) replaced by magnetite. At the localities of the Sierra del Tigre, Sierra de Puerto Nuevo and San Cristóbal chromitite

deposits are hosted in the uppermost part of the dunite section. These chromite deposits are the targets of this study and are described in more detail below. The wehrlites occur as irregular layers, less than 10 m thick, in the upper part of the dunites; they consist of olivine partly replaced by lizardite, pyroxenes and magnetite after chromite. In contrast, the pyroxenites are pockets and dykes of about 10 m dimension that are found above the wehrlites.

The *Critical Zone* is a layered dunite-pyroxenite-gabbro sequence. This unit is observed in the Sierra del Tigre, Sal-Si-Puedes Canyon and San Cristóbal, and consists of up to 100 m of alternating tabular bodies and lenses of dunite, wehrlites (like those described above) pyroxenites and gabbros. The lower part of this zone is dominated by dunite containing bodies of gabbronorite, whereas upwards in the sequence the proportion of gabbronorite increases and it contains small bodies of dunite (Fig. 2). Pegmatoidal pyroxenites are increasingly more abundant from the middle part of this zone to the top of the sequence.

The *Gabbroic Zone* overlies the gabbroic portion of the critical zone described earlier. It includes gabbros, pyroxene gabbro, olivine gabbronorite, gabbronorite (the most common rock type) and ferrograbbros on the top of the sequence (Fig. 2).

A maximum age of Late Triassic has been determined for the mafic-ultramafic rocks by U-Pb dating on zircon from plagiogranites that intrude peridotites in Arroyo San Carlos (221 ± 2 Ma) on the southern flank of the Sierra de San Andrés antiform, and titanite (220 ± 2 Ma) from albitite on top of the gabbroic sequence (Fig. 2; Kimbrough and Moore, 2003, and references therein).

2.3. Chromite deposits

Ninety-seven chromite deposits have been described from the Puerto Nuevo Sequence (Castro-Leyva, et al., 2001; Vatin-Perignon et al., 2000; Radelli, 2008). Most of these deposits were mined (Appendix 1) during the 1980s and they cluster into three mining districts, namely El Tigre, San Agustín and San Cristóbal (Fig. 2).

The El Tigre district is located to the north of the Arroyo del Tigre and comprises the north part of the Sierra del Tigre massif; it contains the largest chromite deposits of the region, with *ca* 6000 tonnes of chromite ore already mined. The El Tigre mining district groups a set of 18 medium-sized (up to 4 m thick and up to 40m

long) chromite deposits with podiform-like, rosary and irregular morphologies (Appendix 1). The long axes of these chromitite bodies are concordant with the mantle foliation of the host peridotite, striking NW80°SE. The San Agustín district includes 6 smaller lenses and tabular bodies of chromitite (up to 2 m thick and 7m long; Appendix 1), also concordant with the foliation of the host peridotite, which strikes NW75°SE but is locally distorted towards NW20°SE by a regional fault. Additionally, abundant fragments and irregular bodies of massive chromitite are scattered at the top of the hills in this area (Appendix 1). The San Cristóbal district is located in the western part of the Arroyo de San Cristóbal and includes 77 medium-sized to small deposits of chromite (from a few centimetres up to 100 metres long) with a wide variety of morphologies that includes podiform, tabular, sill, veins and en-échelon (Appendix 1). These chromitite bodies are both concordant and subconcordant with the foliation of the host peridotite, which strikes NW70°SE.

The chromitite bodies of the three mining districts are systematically hosted by dunites in the uppermost part of the Peridotite Zone, near the Critical Zone. Chromite textures are mainly massive but some bodies show gradations of semi-massive and disseminated-textured ores towards the host dunite (Appendix 1). Chromite grains are unaltered (Appendix 1) and contain inclusions (<50 μm across) of both anhydrous (pyroxene and olivine) and hydrous (amphibole, serpentine, chlorite) silicates, platinum-group minerals (PGM) and very rare base-metal sulphides (BMS). These microstructures and compositions of these mineral inclusions are described in more detail below.

3. SAMPLES

Twenty chromitite samples representative of ten bodies hosted in dunites from the Puerto Nuevo sequence at El Tigre (bodies T1, T2, T3 and T4), San Agustín (bodies SA1 and SA-INDEF) and San Cristóbal (bodies SC1, SC2, SC3 and SC4) were collected for this study. In order to study the petrography of the chromitites and analyse the major-, minor- and trace-element chemistry of chromite and interstitial silicates, we prepared and examined 67 polished thin sections, including 16 massive, 1 semi-massive and 3 disseminated chromitites. These samples were also studied under the scanning electron microscope in an effort to identify homogenous zones in chromite, and silicate and platinum-group mineral (PGM) inclusions suitable for *in*

situ microanalysis. Whole-rock PGE analyses were performed on 19 chromitite samples. A complete list of the samples used in this study is provided in Appendix 2; analytical procedures are described in detail in Appendix 3, and the results are presented in Tables 1 and 2, and the electronic Digital Appendixes 4 to 10.

4. RESULTS

4.1. Geochemistry of chromitite

4.1.1. Chromite chemistry

Electron microprobe analyses of chromite from chromitites of the three mining areas studied in this paper yield Cr_2O_3 contents of 47.6-53.1 wt% with correspondingly high Cr# [(Cr/(Cr+Al) atomic ratio; 0.61-0.69] and TiO_2 <0.21 wt%, which overlap the compositional fields for typical podiform (ophiolitic) chromitites (Fig. 3a-d; Appendix 4). LA-ICP-MS analyses of chromite from the three areas from Puerto Nuevo yielded contents of the minor- and trace-elements that are also similar to those of other high-Cr ophiolitic chromitites (Fig. 6a-h; Appendix 5). They are characterised by small amounts of Sc (<6.2 ppm), Ga (24-41 ppm), Co (179-263 ppm), Zn (307-662 ppm), and higher levels of V (716-1304 ppm), and Mn (977-1445 ppm).

4.1.2. Bulk-rock contents of platinum-group elements

Bulk-rock contents of PGEs are relatively high (312-980 ppb) mainly due a strong enrichment in IPGE (296-930 ppb) relative to PPGE (16-55) (Table 1). This relative abundance of IPGE over PPGE is reflected in an almost continuous strong negative slope from Os to Pd (Pd/Ir = 0.02-0.07) and the lack of a positive Ru anomaly in chondrite-normalised PGE patterns. However, the chromitite samples from San Agustín are characterised by relatively flat segments from Os to Ru (Fig. 5a-f).

4.2. Elemental and isotopic compositions of mineral inclusions in the chromitites

4.2.1. Silicates

The Puerto Nuevo chromites contain sub-micron size needles of pyroxene with preferred crystallographic orientation (Fig. 6a-d). The Energy-Dispersive

Spectroscopy (EDS) spectra obtained using Field-Emission scanning electron microscopy (FESEM) and EMPA analysis on four relatively large grains indicate that the lamellar silicates are diopside and enstatite (Appendix 6 and 7). Furthermore, the measured Raman spectra of pyroxene lamellae within chromite grains have peaks at 141, 231, 325, 360, 394, 667, 856, 1013 and 1048 cm^{-1} (Fig. 6e), which are coincident with those described by Prencipe et al. (2012) for diopside.

These pyroxene lamellae in chromite are accompanied by rare olivine (Mg#= 0.91) and abundant secondary inclusion trails of amphibole (edenite and pargasite), chlorite (clinochlore and penninite) and/or serpentine with variable amounts of MgO (33.9-39.7 wt%), Al_2O_3 (0.4-6.5wt%) and low SiO_2 (34.1-42.7 wt%) and MnO (< 0.08 wt%) (Fig. 5f-g; Appendix 7). The hydrous silicates also constitute the interstitial silicate matrix.

4.2.2. Platinum-group minerals

The remarkable whole-rock enrichment in Os, Ir and Ru has its mineralogical expression in abundant and exceptionally large grains (> 50 μm) of the laurite - erlichmanite (RuS_2 to OsS_2) solid solution series, which are accompanied by smaller grains (< 15 μm) of osmium and irarsite (IrAsS) (Fig.7a-h; Table 2). Most of these grains were found inside chromite grains, and less commonly embedded in the silicate matrix between chromite grains. No differences in morphology or composition were observed among grains located in these different microstructural domains. Most grains of laurite and osmium are homogeneous in composition, although a few larger grains exhibit zoning (Fig.7b-c).

In situ LA-MC-ICP-MS analyses of seventy-six individual grains of PGMs reveal significant differences in the Os-isotope composition among grains within a single thin section, although it is unrelated with the microstructural location of the grains (i.e., inside of chromite or embedded in the silicate matrix; Appendix 8). The $^{187}Re/^{188}Os$ ratio is very low in most grains (<0.013±0.0008; 2σ uncertainty), thus yielding $T_{MA} \approx T_{RD}$ model ages that span between 0.16 and 1.13 Ga and cluster around a single age peak at ~325 Ma (see cumulative age plot in Appendix 8).

4.2.3. Zircons

Thirty-three zircon grains larger than 50 μm were recovered from the Puerto Nuevo chromitites, including 20 from San Cristóbal, 11 from San Agustín and 2 from the El Tigre (Figs. 8, 9, 10; Appendix 9 and 10).

Ten of these zircons are euhedral-elongated grains with internal CL structures characterised by either oscillatory or sector zoning parallel to crystal faces (Fig. 8). *In situ* analyses of these grains yielded concordant or nearly-concordant ages that range between 278 ± 4 and 310 ± 3 Ma (1σ uncertainty) and yield a mean $^{206}Pb/^{238}U$ age of 294 ± 2 Ma (MSWD =1.19 and probability = 0. 31; Fig. 9 and Appendix 9). Most of these euhedral grains are characterised by low $\delta^{18}O$, within or close to the mantle range (<5.3‰ ± 0.6‰; Valley et al., 2005), but two grains have higher values (6.10-7.8). The LA-MC-ICP-MS analyses yielded radiogenic Hf-isotope values corresponding to $\varepsilon_{Hf}(t)$ between +1.8 and +9.1 (Fig. 10a-c; Appendix 9).

The remaining zircons (n=23) are mostly rounded grains with either complex internal CL structures (partly resorbed cores overgrown by rims with no visible arrangement), or cloudy high-luminescence patterns, although a few grains exhibit continuous oscillatory zoning (Fig. 9). *In situ* analyses on 20 of these zircons yielded scattered concordant, sub-concordant and discordant U-Pb ages varying from 467 ± 3 Ma to 2263 ± 44 Ma (Fig. 9; Appendix 9 and 10), with a main cluster composed of 5 analyses at ~ 1150 Ma (i.e., 1152 ± 13 Ma, MSWD =1.2 and probability = 0. 29; Fig. 9 and Appendix 10). All these zircons, irrespectively of their ages (and whether concordant or discordant) have $\delta^{18}O$ higher than the mantle range (5.9-12.4‰) and variable Hf-isotope ratios ($\varepsilon_{Hf}(t)$ from -18.7 to +6.9; Figs. 9 and 10a-c; Appendix 9 and 10). Thus, two main populations can be distinguished on the basis of Hf-isotope compositions (Fig. 10a-c): (1) juvenile $\varepsilon_{Hf}(t)$ (+0.7 to +6.9), which includes most of the Proterozoic zircons (ages between 912 ± 8 Ma and 1283 ± 23 Ma) and one grain 467 ± 3 Ma old; (2) non radiogenic $\varepsilon_{Hf}(t)$ between -0.4 and -18.7 including zircons with ages from 571 ± 8 Ma to 1152 ± 10 Ma.

5. DISCUSSION

5.1. Pyroxene lamellae as evidence of ultrahigh pressure (UHP)

The Puerto Nuevo chromitites contain pyroxene needles with preferred crystallographic orientation in chromite (Fig. 6), a petrographic feature that has been

only observed in chromitites hosted in the mantle section of ophiolites from Tibet and Oman (Yamamoto et al., 2009; Miura et al., 2012; Griffin et al., 2016; Xiong et al., 2017). Recent experiments have demonstrated that magnesiochromite can incorporate only <0.5 wt% CaO at 12-15 GPa and minor amounts of SiO_2 <1-2 wt% at <16 GPa (Wu et al., 2016; Zhang et al., 2017). In contrast, the chromite polymorph with a calcium ferrite structure (CF-type, $CaFe_2O_4$) can accommodate high amounts of SiO_2 (~3-5 wt% at 14-18 GPa in the $MgCr_2O_4$-Mg_2SiO_4 system and up to ~11-14 wt% in the $MgAl_2O_4$-Mg_2SiO_4 system; Wu et al., 2016) and Ca (~7-8 wt% at 14-18 GPa; Wu et al., 2016). These two polymorphs of chromite can coexist at 14-18 GPa and ~1400-1600°C (Zhang et al., 2017), although their relative stability is strongly dependent on the composition of the starting spinel. Thus, Ishii et al. (2014, 2015) observed in their experiments the decomposition of magnesiochromite ($MgCr_2O_4$) to a modified ludwigite-type phase (mLd; $Mg_2Cr_2O_5$) and eskolaite at 12-16 GPa, whereas chromite was observed to transform to CF-type structure at pressures > 12.5 GPa by Chen et al. (2003). All the aforementioned phases will finally transform into an orthorhombic $CaTi_2O_4$ [=CT]-type structure at ~20 GPa (Chen et al., 2003; Zhang et al., 2017). Moreover, the experiments of Wu et al. (2016) and Zhang et al. (2017) indicate that if the "chromite" (re)-crystallises in the stability field of the CT-type phase, it breaks down to mLd+eskolaite during ascent, thus releasing SiO_2 and CaO to the surrounding mantle and precluding the formation of pyroxene lamellae in low-pressure chromites.

The Puerto Nuevo chromitites, like other mantle-hosted chromites with ultra-high pressure (UHP) minerals (e.g., coesite Arai and Miura, 2016, and references therein), do not preserve textures that indicate the presence of these two precursor phases (i.e., mLd and eskolaite), but may still contain pyroxene lamellae. These observations suggest that the chromitites in this study never experienced mantle conditions deeper than those corresponding to the stability field of the calcium-ferrite polymorph which, according to the experimental studies above, is stable in the P-T region between 12.5 and 20 GPa at >1400°C. Moreover, the Puerto Nuevo chromites yielded micro-Raman spectra with positions at 481, 555-581-601, 655 and 697 cm^{-1}, which overlap those of low-pressure cubic chromite and low-to-high pressure magnesiochromites (Fig. 6e). Therefore, we suggest that: (1) CaO and SiO_2 could have been originally present in the high-pressure chromites (either CF-type or

magnesiochromite) and were later redistributed in lower-pressure cubic chromite during the decompression of high-pressure polymorphs, as described in natural samples and experiments, and (2) there could exist micro-scale intergrowths of the different chromite polymorphs within single chromite grains, thus evidencing a rapid decompression and allowing the preservation of an almost complete series of polymorphic changes (e.g., Satsukawa et al., 2015). However, further EDS and TEM studies are required to evaluate the latter possibility.

It is noteworthy that exsolutions of coesite or other minerals of the SuR-UHP assemblage have not been identified in this study. Wu et al. (2016) have demonstrated in their experiments that SiO_2 will exsolve from chromite once CaO and MgO have been completely consumed to form clinopyroxene and $MgSiO_3$. Therefore, the absence of coesite exsolution in the Puerto Nuevo chromitites might simply reflect an incomplete reaction during the polymorphic change of the high-pressure magnesiochromite or CF-type polymorph to low-pressure chromite. It may also suggest that the Puerto Nuevo chromitites followed a different P-T path than the typical Tibetan UHP chromitites, which would be also consistent with the lack of other minerals of the SuR-UHP assemblage (e.g., diamonds). This latter scenario is similar to that reported for UHP chromitites that are concordant with mantle peridotite in the northern part of the Oman ophiolite and from the UHP Higashi-Akaishi peridotite complex in Japan, where chromite grains contain pyroxene lamellae but not minerals of the SuR-UHP assemblage (Arai and Miura, 2016 and references therein). Arai and Miura (2016) have interpreted the latter chromitites as an intermediate case between ordinary low-pressure chromitites and the typical Tibetan UHP chromitites, in which conversion to UHP could take place within the upper mantle and not at the P-T conditions prevailing in the Mantle Transition Zone (MTZ) or its vicinity. Thus, the Puerto Nuevo chromitites are more similar to those that were recycled from the deep upper mantle than to those in ultra-deep-seated environments (i.e., MTZ).

5.2. Origin of hydrous-silicate inclusions in chromite

The Puerto Nuevo chromitites are crosscut by trails of hydrous silicates, including amphibole, chlorite and serpentine (Fig. 6f-g), which clearly postdate the exsolution of the pyroxene lamellae. Experiments indicate that pargasitic amphibole is unstable at >3 GPa and ~1150°C (~100 km depth; Frost, 2006), whereas the high-

pressure serpentine polymorph antigorite is stable at >1.6 GPa but always below ~650°C in the $MgO–Al_2O_3–SiO_2–H_2O$ (MASH) system (Ulmer and Trommsdorff, 1999). These P-T conditions suggest that hydrous silicate trails were formed after UHP metamorphism affected the chromitites. We suggest that different generations of fluid-filled fractures were formed in chromite during instantaneous tension fracturing that affected the chromitites, as happens in mantle peridotites, thus allowing fluid infiltration by crack propagation. These fractures later annealed by re-crystallisation of chromite at subsolidus conditions (600-950 °C; Melcher et al., 1997) during their passage through the shallow mantle. Similar serpentine trails of "shallow mantle origin" have been reported in diamond-bearing chromitite pods of the Luobusa ophiolite (Arai and Miura, 2016).

5.3. Low-pressure geochemical fingerprints in chromitite

The relatively high contents of Cr_2O_3, the low contents of TiO_2 and Fe_2O_3, and the patterns of minor- and trace elements in the Puerto Nuevo chromites are similar to those of high-Cr chromitite pods hosted in the mantle section of supra-subduction zone ophiolites (Figs. 5a-d; 6a-h; 15a-f). Remarkably, the MORB-normalised minor- and trace-element patterns of the Puerto Nuevo chromites are very similar to those of the chromites in low-pressure chromitites from the oceanic supra-subduction zone (SSZ) mantle (Fig. 11a-f). They exhibit slightly different distributions of minor- and trace-element sthan the chromites in the UHP chromitites of the Luobusa ophiolite (Fig. 11d). Moreover, the calculated melts in equilibrium with the Puerto Nuevo high-Cr chromitites overlap those of boninitic-like and high-Mg IAT melts that have crystallised high-Cr chromitites in shallow portions of the oceanic and/or continental mantle of many SSZ ophiolites (Table 3; Appendix 4). Consistently, the Puerto Nuevo chromitites have chondrite-normalised PGE patterns, with Os, Ir, Pt and Pd similar to those reported in such types of chromitites (Fig. 5c, e, f) but slightly different to those reported for the UHP Luobusa chromitites (Fig. 5d). Arai (2013) also noticed differences in the PGE distribution between the Luobusa UHP chromitites and some discordant chromitites from Oman and other ophiolites.

Therefore, the Puerto Nuevo chromitites have geochemical fingerprints for chromite and bulk-rock PGE that are compatible with those of ordinary low-pressure chromitites hosted in the oceanic/continental mantle section of SSZ ophiolites.

5.4. Platinum group minerals

Exceptionally large (> 30 μm) grains of the laurite-erlichmanite (RuS_2-OsS_2) solid-solution series coexist with osmium alloys within chromite grains in the Puerto Nuevo chromitites (Fig. 7a-f). A series of experiments that involve the crystallisation of chromite from basaltic melts (P= 1 bar) have demonstrated that similar Ru-poor osmium alloys and laurite can co-precipitate in equilibrium at ~1275 °C and under relatively low sulphur fugacities (approximately log fS_2= −2; Bockrath et al., 2004). These studies also show that Os solubility in laurite increases with decreasing temperature and/or increasing fS_2. Therefore, the patterns of zoning observed in some laurites at Puerto Nuevo (Fig. 7b-d) indicate that either temperature and/or fS_2 had to be variable in the melt before entrapment of laurite grains by crystallising chromite grains. The mixing (or mingling) of basaltic melts with contrasting physicochemical properties (i.e. different Si contents) would generate a heterogeneous environment with variable temperature and fS_2 that promoted the crystallisation of zoned laurites (González-Jiménez et al., 2009). Melt mixing or mingling is also the most probable mechanism for the genesis of chromitites in the uppermost part of the mantle in SSZ environments (see reviews by González-Jiménez et al., 2014; Arai and Miura, 2016). Also, the exceptionally large size of some laurite grains suggests a very efficient collection of PGEs by chromite crystallising from basaltic melts (O'Driscoll and González-Jiménez, 2016). Alternatively, such characteristics may imply the entrainment of basaltic melt(s) that were particularly enriched in PGEs (Petrou and Economou-Eliopoulos, 2009). This is consistent with the crystallisation of the Puerto Nuevo chromitites from high-Mg basaltic melts of boninitic affinity in a SSZ (e.g., Prichard et al., 2008).

Further, some of the biphasic grains of laurite + Os-Ir alloys are associated with pyroxene lamellae in chromite (Fig. 7e-f). Griffin et al. (2016) observed similar PGM-silicate assemblages in the UHP Luobusa chromitites. They suggested that PGM grains originally formed at low pressures and were nucleation points for the exsolution of diopside as high-pressure polymorphs (either CF-type phase or high-pressure magnesiochromite) inverted to low-pressure cubic chromite. Following this model, the low-pressure magmatic PGM assemblages must have remained unscathed during the different polymorphic changes that affected their host chromite.

Considering that high-pressure magnesiochromite becomes stable at ~1350°C and ~12 GPa (Zhang et al., 2017) the 'survival' of the laurite + Os-Ir assemblages appears to be inconsistent with the replacement of laurite by Ru-(Os-Ir) alloys at > 1275°C (Fonseca et al., 2012). The preservation of laurite and Os-Ir alloys in UHP chromitites from both Puerto Nuevo and Tibet may reflect the effect of high pressure in counterbalancing the Ru-(Os-Ir) sulphide/alloy equilibrium. It might also explain why PGM encased in the chromitite from both localities yield T_{RD} ages that are consistent with known geological events —Puerto Nuevo PGM yielded T_{RD} ages with a clear peak at 325 Ma that roughly correlates with the magmatic event at *ca* 300 Ma recorded in PGMs from ultramafic complexes in California (Pearson et al., 2007) and the Loma Baya chromite deposit in SW Mexico (González-Jiménez et al., 2017b). Similarly, laurites of the UHP Luobusa chromitites yield T_{RD} ages similar to coexisting metasomatic zircons (McGowan et al., 2015). Therefore, PGMs encapsulated in chromite (an oxide with negligible Os contents) would keep their Re-Os system undisturbed, even at high temperatures and pressures, unless these minerals reacted with an external high-temperature Os-bearing fluid or melt (González-Jiménez et al., 2012).

5.5. Origin and provenance of chromitite zircons

Belousova et al. (2015) suggested that inherited zircons in chromitites and host peridotites of the Coolac Belt in SE Australia were physically incorporated during the injection of granite-related melts/fluids nearby. However, the plagiogranites that intrude the ultramafic rocks of the Puerto Nuevo sequence have a single population of zircons (U-Pb) at ~221 Ma (Kimbrough and Moore, 2003). Moreover, zircons of Mesozoic granitic rocks associated with the ultramafic rocks of the Puerto Nuevo sequence yield much younger U-Pb ages, and Hf and O isotopic compositions distinct from those studied in this paper (Shaw et al., 2014 and references therein). Thus, it is unlikely that zircons in the chromitite with ages over ~294 Ma were physically incorporated from younger intruding rocks.

Zircons with U-Pb ages ranging between Early Proterozoic (2263 ± 44 Ma) and Ordovician (467 ± 3 Ma) exhibit large variations in $\varepsilon_{Hf}(t)$ (between -18.7 and +6) and $\delta^{18}O$ values (between 5.9 and 12.4‰) that are much higher than those of the normal mantle (Figs. 8, 9 and 10; Appendix 9 and 10). Many of these zircons are

abraded or well-rounded grains that have residual cores with overgrowths (Fig. 8), suggesting a detrital history with several events of corrosion during transport in sedimentary settings and/or dissolution/(re)-crystallisation during magmatic and/or metamorphic events. Their ages and Hf and O isotopic compositions broadly match the age distribution of zircons in neighbouring continental crust in southern North America (Fig. 9 and references in Appendix 11).

In contrast, the well-developed external faces of the subset of zircons that yield an age peak of ~294 Ma (Fig. 9) suggest that these were not subjected to such intensive abrasion as the xenocrystic zircons described above (e.g., Rojas-Agramonte et al., 2016). As there are no signs of secondary alteration or metamictisation that would reset the U-Pb isotopic system, the inferred crystallisation age (*ca* 294 Ma) is interpreted to be the maximum possible age of the formation of the chromitites in the SSZ mantle. All these zircons, except two, yielded almost identical low $\delta^{18}O$ and positive $\varepsilon_{Hf}(t)$ values, suggesting derivation from a mantle-like source. This may reflect an origin related to melts/fluids that contributed to the formation of either mafic oceanic or continental crust. A possible source for these zircons could be undeformed felsic to mafic igneous rocks that were dated by U-Pb zircon geochronology between 311 and 255 Ma, and which intrude different units of the Palaeozoic Oaxacan and Acatlán complexes in southwestern Mexico. For example, zircons from two of these magmatic units (Cuanana pluton and Honduras batholith; dated at 290-311 Ma) have $\varepsilon_{Hf}(t)$ values (between +3.8 and +7.6) that overlap those of the chromitite zircons reported here (Fig. 10 and Appendix 9; Ortega-Obregón et al., 2014).

Further, zircon age distributions comparable to those from the studied chromitites have been described in the Arteaga Complex (Fig. 9), which is interpreted as part of a submarine sedimentary fan (the Potosí Fan) with sedimentary sources in the former Oaxaquia subcontinental block and their Carboniferous-Permian continental arc-related igneous rocks (Centeno-García, 2017 and references therein). Rocks of the Arteaga Complex underwent subduction beneath a west-facing intra-oceanic arc that extended along western Mexico since the Early Triassic (~ 250 Ma; Centeno-García, 2017). Therefore, zircons in the Puerto Nuevo chromitites could represent remnants of partly digested continental crust or continent-derived sediments

in oceanic crust delivered into the mantle via subduction of the Potosí Fan (e.g., Rojas-Agramonte et al., 2016).

5.6. Chromitite formation in a mantle wedge polluted with crustal material

Yamamoto et al. (2013) explained the presence of crustal zircons in the UHP Luobusa chromitites as the result of the initial formation of chromitites at low pressures in a supra-subduction zone mantle peridotite wedge "polluted" with crustal material. Crustal contamination of the mantle wedges above supra-subduction zones can be produced by (1) oceanic crust and sediments dragged down by the subducting slab (Rojas-Agramonte et al., 2016), (2) subduction erosion of the fore-arc regions (Scholl and von Huene, 2009), or (3) delamination of dense, thickened lower crust beneath a volcanic arc (Zandt et al., 2004). Although at this stage of research the latter two options cannot be ruled out, the occurrence of inherited zircons in the Puerto Nuevo chromitites, with provenances from varied crustal blocks and complex detrital history, suggests that these were part of sediments that were incorporated into the upper mantle via subduction.

Subducted slabs can transport significant volumes of sediments to depths greater than 50 km (Scholl and von Huene, 2007) and these, in turn, may be transferred to the mantle wedge by (1) fluids/melts channelised in melt conduits or fractures (González-Jiménez et al., 2017a), and/or (2) detachment and buoyancy-driven diapiric upflow of plumes of slab-derived sediments (Gerya and Yuen, 2003).

The first mechanism links the transfer of slab-derived zircons to the introduction of silica- and alkali-rich fluids/melts due to the dehydration/anatexis of subducted sediments through fractures in mantle peridotites. This may result in a suite of metasomatic veins and dykes of pyroxenite and amphibole-rich rocks (Berly et al., 2006; Marocchi et al., 2010; Grant et al., 2016) that may also incorporate relict zircons (Gebauer, 1996; Zanetti et al., 2016; González-Jiménez et al., 2017a).

The second mechanism is based on petrological-thermomechanical subduction models that predict the formation of large ascending diapirs ("cold plumes"; Gerya and Yuen, 2003) in the mantle wedge as a result of Raleigh-Taylor instabilities caused by hydration and melting in the upper surface of subducting slabs. Cold plumes can be present in all types of subduction zones and consist of partly molten crustal (including sediments, continental crust and basalts) and mantle rocks

mixed on length scales from a few tens of metres to hundreds of kilometres (e.g., Castro et al., 2010; Blanco-Quintero et al., 2011; Castro, 2014). Laboratory experiments indicate that cold plumes initially develop as ascending plumes that may become stationary and underplated on a time scale of several million years (e.g., Sizova et al., 2009). At the interface of the cold plume with the surrounding mantle, reaction with peridotites results in hybrid pyroxene- and/or amphibole-rich rock shields that prevent further reaction, making it possible for the plumes to survive in the mantle for a long time (e.g., Castro et al., 2010). Sizova et al. (2009) and Castro et al. (2010) have demonstrated that temperatures in ascending and stationary plumes usually do not exceed 900°C, which is close to the blocking temperature of zircon (> 900 °C; Cherniak and Watson, 2000). Therefore, these relatively cool plumes offer a mechanism by which zircon xenocrysts with a wide spectrum of ages and Hf- and O-isotope compositions can be transferred from the slab to the mantle wedge.

The geochemical composition of the Puerto Nuevo chromitites indicates that they precipitated from melts akin to high-Mg IAT and boninites (Table 3 and Appendix 11). Pulses of SiO_2-undersaturated high-Mg IAT melts that migrate through the mantle may promote consumption of pyroxenes from peridotites, thus generating dunite sheaths and a secondary melt with a local boninitic affinity, according to the following reaction: SiO_2-poor melt + pyroxenes + hydrous phases $\rightarrow$ olivine + SiO_2-rich melt (Arai and Miura, 2016). A continuous supply of batches of primitive SiO_2-undersaturated melt may produce a self-sustaining system with mixing of melts with variable degrees of fractionation enabling the precipitation of chromite within the dunite channels (González-Jiménez et al., 2011, 2014).

Considering the two scenarios proposed above for the transfer of crustal material from the slab to the mantle wedge, the more SiO_2-rich component in the parental melts of the chromitite could also be (1) the more silica- and alkali-rich melt/fluid migrating through melt conduits, or (2) pre-existing pyroxenites (or their derived partial melts) that precipitated from hybrid mafic melts with a significant contribution of crustal sediments (e.g., Marchesi et al., 2012). The mixing of these two components at a new transition of the melt composition (i.e., from SiO_2-undersaturated to SiO_2-richer) may have significantly lowered the solubility of Cr in the primitive high-Mg IAT, thus triggering the precipitation of chromite (Bédard and Hérbert, 1998). The segregation of pyroxene (or pyroxenites) would then follow, as

observed in many low-pressure chromitites elsewhere (e.g., Zanetti et al., 2016). At Puerto Nuevo, these pyroxene components are apparently absent, thus suggesting that pyroxenes would have dissolved into chromite (or into its HP polymorphs) during high-pressure metamorphism, and later reappeared as pyroxene lamellae exsolved from low-pressure chromite when decompressed en route to the surface (Arai, 2013).

In the proposed model, chromitite crystallising from the hybrid melts that were generated by melt-melt or melt-rock interaction/assimilation would inherit the old zircons from (1) acid/hybrid melts channelised through melt conduits or fractures, or (2) more likely from partial melting/assimilation of pre-existing zircon-bearing pyroxenites (or their derived partial melts), either veining the mantle or forming the external shield of cold plumes. González-Jiménez et al. (2017a) have recently noted that chromitites that crystallised within melt conduits in the SCLM of the Ronda massif contain "crustal" zircons transported by melts with a secondary boninitic affinity. The latter melts were also generated as a result of (1) hybridisation of primitive SiO_2-undersaturated basaltic melts with fluids/melts derived from the dehydration/anatexis of subducted metasediments, and (2) partial melting of pre-existing zircon-bearing pyroxenites corresponding to UHP recycled crustal material in the mantle.

5.7. Tectonic scenario for the deep mantle recycling of the chromitite

The structure of the present margin of western North America in Mexico is the result of the accretion of several convergent-basin complexes between the Late Palaeozoic and the Mesozoic (e.g., Busby, 2004). During the Late Carboniferous-Early Permian the northwestern boundary of Gondwana in northwestern Mexico developed as a passive and/or trailing margin (Centeno-García, 2017 and references therein). This continental crust of Proterozoic (mainly Grenville) age was intruded by a series of Late Palaeozoic to Triassic age (311-232 Ma) granitoids, which are interpreted as part of a continental magmatic arc that extended from the southwestern USA, through Mexico and Guatemala into the Northern Andes in Colombia (Fig; 12a-c). The upper volcanic-sedimentary levels of this continental arc were not preserved in Mexico, but the belt of granitoids crosscuts and links the Pennsylvanian-Early Permian units of the North American craton (Chihuahua and Sonora) with the Coahuila, Maya, Chortis and Sierra Madre terranes. The onset of this magmatism in

the western margin of Gondwana was roughly coeval with the mid-Permian cessation of Gondwana-North America convergence that led to the formation of Pangea along the Ouachita-Marathon suture at *ca* 290 Ma (Centeno-García, 2017). It also marks a change in the tectonics of Mexico from being dominated by circum-Atlantic collision to the accretionary tectonics of circum-Pacific terranes. Therefore, it records the subduction of oceanic lithosphere of one or more plates of the Paleo-Pacific basin that initially lay beneath western margin of Gondwana, and later, beneath western Pangea (Ortega-Obregón et al., 2014, and references therein). Apparently, this subduction and the associated magmatic ceased drastically *ca* 270 Ma ago at the geographic location of the peninsula (Solari et al., 2001) whereas the former Pacific margin of Oaxaquia evolved into a passive margin. Then, a large submarine fan developed along the western margin of Oaxaquia between the Middle and Late Triassic time (i.e., the Potosí Fan; Centeno-García et al., 2017). Regional stratigraphic relationships suggest that the distal facies of the Potosí Fan was deposited in a marginal ocean basin known as the Arteaga basin. Rocks of the Arteaga Complex underwent subduction along western margin of Mexico from Early Triassic to Middle Jurassic (Kimbrough and Moore, 2003; Busby, 2004; Centeno-García, 2017). According to Centeno-García (2017), the subduction zone that consumed the oceanic crust of the Arteaga Basin and its sedimentary cover (the Potosí Fan) dipped under the intra-oceanic arc to the west. This model is supported by the occurrence of volcanic rocks with island-arc affinity (IAT, andesitic and MORB) in the San Hipólito Formation and blocks of basalts with similar arc affinity within the Las Ollas Complex in the Guerrero Composite Terrane in SW Mexico (Kimbrough and Moore, 2003; Busby, 2004; Talavera-Mendoza, 2005; Centeno-García et al., 2017).

Figure 12 shows a possible scenario for the formation and evolution of the Puerto Nuevo chromitites within the evolution of the paleo-margin of western North America. During the Early Triassic the northwestern boundary of Pangea developed as a passive margin once the Late Permian to Early Triassic continental arc magmatism waned (Fig. 12a-b). The erosion of the Precambrian to Palaeozoic rocks produced large volumes of sediments that were later deposited on the western edge of the platform and in the submarine Potosí Fan in the Paleo-Pacific Arteaga oceanic basin (Fig. 12a-b). Sediments that included the crustally-derived zircons of the oceanic basin were dragged into the mantle by subduction, thus contaminating the supra-subduction mantle wedge —either transferred to the mantle wedge by

fluid/melts channelised through fractures and/or by means of diapiric upflow. The dehydration of the subducted slab released large volume of fluids that promoted hydrous partial melting of mantle-wedge peridotite, thus generating primitive basaltic melts. Once these ascending melts crossed the overlying mantle wedge polluted with crustal material or the hybrid products of crustal contamination (e.g., pyroxenites), they became more enriched in silica and consequently generated hybrid mafic melts with the ability to crystallize chromitites (Fig. 12b). Such processes roughly coincide with the start of subduction at *ca* 250 Ma and thus the subduction zone began to be fed with sediments. In this scenario, some continental zircons already present in the supra-subduction mantle wedge were incorporated into chromitite as a result of melt-melt and melt-rock interaction. Zircon could have been already present in the hybrid rocks formed shortly before chromitites, or could have been rapidly captured by early minerals that formed from the same parental melts as chromitites (e.g., chromite, olivine, pyroxene), thus preventing their dissolution in mafic melts (Jiang et al., 2012).

Meanwhile, PGM originally formed as liquidus phases from the same parental melt were mechanically trapped during the precipitation of chromite, thus inheriting the Os isotope values of older melting events in the mantle. The Os-isotope model ages of 1.13 Ga overlap the period of construction of the Oaxaquian continental crust during the Grenvillian orogeny. In contrast, the model age peak at ~ 325 Ma reflects melt depletion in the mantle associated with the formation of the continental magmatic arc in the western Mexico *ca* 311-232 Ma ago. The input of mantle melts during the construction of the Carboniferous-Permian continental crust is recorded in the positive $\varepsilon_{Hf}(t)$ and low $\delta^{18}O$ values of the Late Carboniferous to Early Permian granite-derived zircons (Ortega-Obregón et al., 2014) and their equivalent populations of idiomorphic zircons in the Puerto Nuevo chromitites (Figs. 8, 9 and 10; Appendix 9).These observations suggest that Proterozoic SCLM underlying the continental crust of Oaxaquia was unroofed and altered during the Mesozoic, thus contributing to the generation of new oceanic lithosphere. The latter would have been the basement for the development of the Arteaga basin and the Vizcaíno intra-oceanic arc.

During the Late Triassic (Ladinian-Carnian) the large-scale downward flow of the mantle convection drove chromitites (and possibly host peridotites) down into the deeper mantle. Numerical simulations ((McGowan et al., 2015; Griffin et al., 2016)

and empirical observations (Xiong et al., 2017) have demonstrated that a significant volume of SSZ mantle peridotites can be carried downward along with the slab in this way. During progressive UHP metamorphism of the low-pressure chromitites, silicate inclusions in chromite (e.g., pyroxenes) that were formed at low pressures were subsequently dissolved in the UHP chromite polymorph(s) while PGMs and zircon remained unscathed. After a period of extension that ended at about the Carnian-Norian boundary, the intra-arc marginal basin of San Hipólito was developed (Fig 18c-d; Kimbrough and Moore, 2003; Busby, 2004). This extension was possibly driven by downward penetration of the slab into the mantle and its rollback, which led to the formation of a low-viscosity upwelling channel (Griffin et al., 2016 and references therein) that allowed the exhumation of deep-seated recycled chromitites (Fig. 12c). During this uplift, the high-pressure polymorph(s) of chromite reverted back to the low-pressure cubic phase while pyroxene lamellae were exsolved from the chromite. The recycled chromitites that contained the record of UHP metamorphism reappeared beneath the spreading centre as part of a mantle diapir. During their exhumation through the shallow mantle, the recycled chromitites were veined by melts/fluids that generated late trails of hydrous silicates, which postdate the exsolution of pyroxenes in chromite. Finally, the peridotites that formed such mantle diapirs constituted the basis of the new oceanic lithosphere that includes the future Puerto Nuevo ophiolite (Fig. 12c-d). The crustal section of this ophiolite was developed during the formation of the San Hipólito marginal basin. It consists of gabbros and pillow lavas with fossiliferous sediments of the San San Hipólito Formation, dated at 221 ± 9 Ma, that overlie the chromitie-bearing peridotite, and the contemporaneous intrusion of dykes of plagiogranites (Figs. 2 and 12c).

6. CONCLUSIONS

The Puerto Nuevo podiform chromitites preserve evidence for both low- and high-pressure assemblages, in this order of formation. Evidence for a shallow origin includes:

(1) the geochemical composition (major-, minor- and trace elements) in chromite and bulk-rock PGEs, which are similar to ordinary low-pressure chromitites that crystallised from arc-type basaltic melts that overlap IAT and boninites, and are found in both the oceanic and

continental mantle sections of ophiolites in supra-subduction zones (SSZ),

(2) PGM assemblages dominated by inclusions of laurite-erlichmanite, Os-Ir alloys and sulpharsenides, which are typically formed from S-undersaturated basaltic melts generated in the SSZ mantle,

(3) the Re-Os signatures of the PGM that, despite the UHP conditions experienced by the host chromites, remain undisturbed and yield Os-model ages that are consistent with known geological events,

(4) xenocrystic zircons of crustal origin derived from nearby crustal terranes.

Evidence for the deep recycling in the mantle of the Puerto Nuevo includes the presence of (1) oriented pyroxene lamellae encapsulated in chromite, and (2) chromite micro-Raman spectra that overlap those of magnesiochromite synthesised in high-pressure and high-temperature experiments. The lack of coesite and other minerals of the SuR-UHP assemblage (e.g., diamonds) in the Puerto Nuevo chromitites parallels those in the northern part of the Oman ophiolite and the UHP Higashi-Akaishi peridotite complex in Japan, which these experienced UHP conditions while in the upper mantle (not in the Mantle Transition Zone, as in the UHP Tibetan chromitites). Further, magmatic (amphibole) and low-temperature (chlorite and serpentine) hydrous silicates in the Puerto Nuevo chromitite postdate the polymorphic changes in chromite and the subsequent formation of pyroxene lamellae.

The above observations rule out previous interpretations of the Puerto Nuevo chromitites as layers of cumulate chromite associated with a mafic-ultramafic body that intruded the continental crust (Vatin-Perignon et al., 2000; Radelli, 2008). Instead, the Puerto Nuevo chromitites were formed in the SSZ mantle wedge beneath an intra-oceanic arc, which underwent deep recycling in the mantle, and finally was exhumed in an intra-arc spreading centre.

ACKNOWLEDGEMENTS

Funding for this research was provided through the CONACyT research project number 155662 and internal budget of the Instituto de Geología (UNAM) to AC, the Ramón y Cajal Fellowship RYC-2015-17596 to JMGJ, and by the project CGL2015-65824-P granted by the Spanish “Ministerio de Economía y

Competitividad" to JAP. Additional funding for chromite microanalyses were provided by the DGAPA-UNAM postdoctoral fellowship to VC. This is also a contribution from the ARC National Key Centre for Geochemical Evolution and Metallogeny of Continents (www.es.mq.edu.au/ GEMOC) and the ARC Centre of Excellence for Core to Crust Fluid Systems. The SHRIMP facility lab and technical staff at Curtin University are also thanked for their support in the data acquisition. We also thank to Carlos Linares (Petrology Laboratory of the, UNAM, Mexico) for his help with the EMPA analyses on chromite. Michelangelo Martini, Luis Abel Jiménez-Galindo and all the personnel at the Fishermen's Cooperative Society at Bahía Tortugas (Baja California Sur) are wholeheartedly thanked for their kind assistance during our fieldwork.

FIGURE CAPTIONS

Figure 1. Regional geological sketch map of the Peninsula based on Castro-Leyva et al. (2001) and Kimbrough and Moore (2003), showing the studied area.

Figure 2. Geological map of the studied area in the northern part of the Peninsula showing the location of the chromite deposits studied in this study and the pseudostratigraphy of the Puerto Nuevo Sequence. The map and the stratigraphic column are based on Castro-Leyva et al. (2001).

Figure 3. Chemistry of primary chromites from Puerto Nuevo chromitites as compared to chromian spinel from various tectonic settings in terms of (a) Al_2O_3 *vs* Cr_2O_3, (b) TiO_2 *vs* Cr_2O_3. (c) Cr# [Cr/(Cr+Al) atomic ratio] *vs* Mg# [Mg/(Mg+Fe) atomic ratio] and (d) Al-Cr-Fe^{3+} compositions. Data sources for chromian spinel of different tectonic settings are Bonavia et al. (1993), Kamenetsky et al. (2001) and Proenza et al. (2007). Legend is inset in the figure.

Figure 4. Compositional variation in terms of Cr# *vs* Ti, Ni, V, Co, Zn, Mn, Sc and Ga in chromites from the Puerto Nuevo chromitites. Data sources are listed in Appendix 11.

Figure 5. C1-chondrite (Naldrett and Duke 1980) normalised patterns of the Puerto Nuevo chromitites and comparison with chromitites from different crustal settings and hosted in the mantle section of ophiolites: (a) chromitites in Ural-Alaskan-type complexes (Garuti et al.,2005) of the Urals and the Bushveld (UG2) Layered Complex (Naldrett et al. 2011), (b) banded chromitites hosted in the oceanic mantle of suprasubduction ophiolites (Pedersen et al., 1993; Economou-Eliopoulos, 2010), (c) and (d) podiform-type chromitites of low-pressure (LP) and high-pressure (HP) origin hosted in the oceanic or continental mantle of suprasubduction zone ophiolites (Economou, 1993; Melcher et al., 1997; Arai, 2013, and references therein), (e) and (f) podiform-type chromitites hosted in the subcontinental

lithospheric mantle (SCLM) of suprasubduction zone and continental margin ophiolites (Grieco et al., 2006; Zaccarini et al., 2004, and references therein). Legend is inset in the figure.

Figure 6. Raman spectra of chromite and diopside lamellae inclusions in the Puerto Nuevo chromitites. Spectra of chromite and magnesiochromite from natural examples and experimental works are shown by comparison. The spectrum for high-pressure chromite polymorph (Chr-12 GPa, 1600°C) is from Zhang et al. (2017).

Figure 7. Backscattered electron (BSE) images of representative platinum-group mineral assemblages in the Puerto Nuevo chromitites: (a to d) euhedral laurite grains hosted in unaltered chromite, (e and f) composite assemblages including osmium in unaltered chromite, (g and h) euhedral grains of osmium released to the interstitial silicate matrix.

Figure 8. Cathodoluminescence (CL) images of representative zircon grains from the Puerto Nuevo chromitites.

Figure 9. Probability density plot showing comparison of U/Pb zircon ages of zircon grains recovered from the Puerto Nuevo chromitites compared with zircons ages from magmatic, metamorphic and sedimentary rocks from Mexican terranes (note that zircons with ages older than the Carboniferous-Permian continental magmatic arc intruding these crustal terranes were not included). Data sources are listed in Appendix 11.

Figure 10. Hf and O isotopic composition of zircons recovered from the Puerto Nuevo chromitites: (a and b) $\delta^{18}O$ and $\varepsilon_{Hf}(t)$ *vs* age, (c) $\delta^{18}O$ *vs* $\varepsilon_{Hf}(t)$. Legend is inset in the figure.

Figure 11. Spider diagrams showing the composition of minor and trace elements of chromites from chromitites of the three mining districts at Puerto Nuevo (a-c) and comparison with other representative low- and high-pressure chromitites from fore-arc and back-arc regions of supra-subduction zone ophiolites (d-f). Data sources for low-pressure chromitites are Thetford Mines (Pagé and Barnes, 2009) and Sagua de Tánamo (González-Jiménez et al., 2015), and for high-pressure chromitite are Luobusa (Zhou et al., 2014). Data sources for high-Cr chromitites from the supra-subduction zone mantle-hosted podiform chromitite array, komatiites and layered continental intrusions are the same of Figure 4.

Figure 12. An illustration of the evolution of the northwestern Mexico showing the formation, deep recycling and final exhumation of the Puerto Nuevo chromitites (after Centeno-García, 2017). (a and b) The northwestern part of Pangea was a passive margin where exhumed crustal terranes were eroded and produced large volumes of sediments that were deposited at the edge of the continental block and by the Potosí submarine fan in the Arteaga oceanic basin. The beginning of the subduction of the Arteaga oceanic lithosphere beneath the Paleo-Pacific oceanic plate led to the formation of the intra-oceanic arc; former sediments of the oceanic basin

were already and being subducted and the mantle wedge was metasomatised by crustal derived fluids/materials; chromitites were formed in this polluted mantle, thus inheriting old recycled crustal zircons. (c and d) Low-P igneous chromitites were converted to UHP chromitites via dragging by subducting slab/mantle convection during the Ladinian-Carnian, whereas a period of extension that ended in the Carnian-Norian was associated with slab-roll back and generated a low-viscosity upwelling channel that exhumed deep-seated chromitites in the San Hipólito intra-arc marginal basin.

TABLES

Table 1. Platinum-group elements of chromitite samples from Puerto Nuevo (in ppb).

Table 2. Representative analyses of platinum-group from the Puerto Nuevo chromitites.

Table 3. Melts in equilibrium with the Puerto Nuevo chromitites.

References

Akbulut, M., González-Jiménez, J.M., Griffin, W.L., Belousova, E., O'Reilly, S.Y., McGowan, N.M., Pearson, N.J., 2016. Tracing ancient events in the lithoshperic mantle: A case study from ophiolitic chromitites SW Turkey. Journal of Asian Earth Sciences 119, 1-19.

Akmaz, R.M., Uysal, I., Saka, S., 2014. Compositional variations of chromite and solid inclusions in ophiolitic chromitites from the southeastern Turkey: implications for chromitite genesis. Ore Geology Reviews 58, 208–224.

Arai, S., 2013. Conversion of low-pressure chromitites to ultrahigh-pressure chromitites by deep recycling: a good inference. Earth and Planetary Science Letters 379, 81–87.

Arai, S. Miura, M., 2016. Formation and modification of chromitites in the mantle. Lithos 264, 277-295.

Augé, T., 1987. Chromite deposits in the northern Oman ophiolite: mineralogical constraints. Mineralium Deposita 22, 1–10.

Avcı, E., Uysal, I., Akmaz, R.M., Saka, S., 2017. Ophiolitic chromitites from the Kızılyüksek area of the Pozantı-Karsantı ophiolite (Adana, southern Turkey): Implication for crystallization from a fractionated boninitic melt. Ore Geology Reviews In press.

Bédard, J.H., Hébert, R., 1998. Formation of chromitites by assimilation of crustal pyroxenites and gabbros into peridotitic intrusions: North Arm Mountain massif, Bay of Islands ophiolite, Newfoundland, Canada. Journal of Geophysical Research 103, 5165–5184.

Belousova, E. A., González Jiménez, J. M., Graham, I., Griffin, W. L., O'Reilly, S. Y., Pearson, N., Martin, L., Craven, S., 2015. The enigma of crustal zircons in upper mantle rocks: clues from the Coolac ultramafic complex, SE Australia. Geology 43, 123–126.

Berly, T., Hermann, J., Arculus, R.J., Lapierre, H., 2006. Supra-subduction zone pyroxenites from San Jorge and Santa Isabel (Solomon Islands). Journal of Petrology 47, 1531–1555.

Blanco-Quintero, I.F., Gerya, T.V., García-Casco, A., Castro, A., 2011. Subduction of young oceanic plates: a numerical study with application to aborted thermal-chemical plumes. Geochemistry, Geophysics, Geosystems 12, Q10012, doi:10.1029/2011GC003717.

Bockrath, C., Ballhaus, C., Holzheid, A., 2004. Stabilities of laurite RuS_2 and monosulphide liquid solution at magmatic temperature. Chemical Geology 208, 265–271.

Bonavia, F.F., Diella, V., Ferrario, A., 1993. Precambrian podiform chromitites from Kenticha Hill, southern Ethiopia. Economic Geology 88, 198-202.

Busby, C., 2004. Continental growth at convergent margins facing large ocean basins: a case study from Mesozoic convergent-margin basins of Baja California, Mexico. Tectonophysics 392, 241-277.

Castro, A., 2014. The off-crust origin of granite batholiths. Geoscience Frontiers. doi: 10.1016/j.gsf.2013.06.006.

Castro, A., Gerya, T., García-Casco, A., Fernández, C., Días-Alvarado, J., Moreno-Ventas, I., Loew, I., 2010. Melting relations of MORB-sediment mélange in underplated wedge plumes: implications for the origin of Cordilleran type batholiths. Journal of Petrology 51, 1267-1295.

Castro-Leyva, T., Delgado-Argote, L.A., GArcía-Abdeslem, J., 2001. Geología y magnetometría del complejo máfico-ultramáfico Puerto Nuevo en el area de San Miguel, Península de , Baja California Sur. Geos 21 (1), 3-21.

Centeno-García, E., 2017. Mesozoic tectono-magmatic evolution of Mexico: An overview. Ore Geology Reviews 81, 1035-1052.

Chen, M., Shu, J., Mao, H.K., Xie, X., Hemley, R.J., 2003. Natural occurrence and synthesis of two newpostspinel polymorphs of chromite. Proceedings of the National Academy of Sciences 100 (25), 14651–14654.

Cherniak, D.J., Watson, E.B., 2000. Pb diffusion in zircon. Chemical Geology 172, 5-24.

Economou-Eliopoulos, M., 2010. Platinum-group elements (PGE) in various geotectonic settings: opportunities and risks. Hellenic Journal of Geosciences 45, 65-82.

Fan, J., Kerrich, R., 1997. Geochemical characteristics of aluminium depleted and undepleted komatiites and HREE-enriched low-Ti tholeiites, western Abitibi greenstone belt– a heterogeneous mantle plume convergent margin environment. Geochemica et Cosmochimica Acta 61, 4723-4744.

Fonseca, R.O.C., Laurenz, V., Mallmann, G., Luguet, A., Hoehne, N., Jochum, K.P., 2012. New constrains on the genesis and long-term stability of Os-rich alloys in the Earth's mantle. Geochimica et Cosmochimica Acta 87, 227–242

Garuti, G., Pushkarev, E., Zaccarini, F., 2005. Diversity of chromite-PGE mineralization in ultramafic complexes of the Urals. In: Törmänen, T.O., Alapieti, T.T. (Eds.), Platinum-group elements—from genesis to beneficiation and environmental impact. Tenth Int. Platinum Symp. (Oulu), pp. 341–344.

Gerya, T.V., Yuen, D.., 2003. Rayleigh–Taylor instabilities from hydration and melting propel ‘cold plumes’ at subduction zones, Earth and Planetary Science Letters 212, 47-62.

Ghosh, B., Pal, T., Bhattacharya, A., Das, D., 2009. Petrogenetic implications of ophiolitic chromite from Rutland Island, Andaman – a boninitic parentage in supra-subduction setting. Mineralogy and Petrology 96, 59-70.

González-Jiménez., J.M., Gervilla, F., Proenza, J.A., Kerestedjian, T., Augé, T., Bailly, L. Zoning of laurite (RuS_2)-erlichmanite (OsS_2): implications for the genesis of PGM in ophiolite chromitites. 2009. European Journal of Mineralogy 21, 2, 419-432.

González-Jiménez., J.M., Proenza, J.A., Gervilla, F., Melgarejo, J.C., Blanco-Moreno, J.A. Ruiz-Sánchez, R., Griffin, W.L. High-Cr and high-Al chromitites from the Sagua de Tánamo district, Mayarí-Cristal Ophiolitic Massif (eastern Cuba): constraints on their origin from mineralogy and geochemistry of chromian spinel and platinum-group elements. Lithos 125, 101-121.

González-Jiménez, J.M., Griffin, W.L., Gervilla, F., Kerestedjian, T.N., O'Reilly, S.Y., Proenza, J.A., Pearson, N.J., Sergeeva, I. 2012. Metamorphism disturbs the Re-Os signatures of platinum-group minerals in ophiolite chromitites. Geology. doi:10.1130/G33064.1.

González-Jiménez, J.M., Griffin, W.L., Proenza, J.A., Gervilla, F., O'Reilly, S.Y., Akbulut, M., Pearson, N.J., Arai, S., 2014. Chromitites in ophiolites: How, where, when, why? Part II. The crystallisatio of chromitites. Lithos 189, 140–158. http://dx.doi.org/10.1016/j.lithos.2013.09.008.

González-Jiménez, J.M., Locmelis, M., Belousova, E., Griffin, William L., Gervilla, F., Kerestedjian, T., O'Reilly, S.Y., Sergeeva, I., Pearson, N.J., 2015. Genesis and tectonic implications of podiform chromitites in the metamorphosed Ultramafic Massif of Dobromirtsi (Bulgaria). Gondwana Res. 27, 555–574.

González-Jiménez, J.M., Marchesi, C., Griffin, W.L., Gervilla, F., Belousova, E., Garrido, C.J., Romero, R., Talavera, C., Leisen, M., O'Reilly, S.Y., Barra, F., Martin, L., 2017a. Zircon recycling and crystallization during formation of chromite- and Ni-arsenide ores in the subcontinental lithospheric mantle (Serranía de Ronda, Spain). DOI: 10.1016/j.oregeorev.2017.02.012.

González-Jiménez, JM., Proenza, J.A., Martini M., Camprubí, A., Griffin, W.L., O'Reilly S.Y., Pearson, N.J., 2017b. Deposits associated with ultramafic-mafic complexes in Mexico: the Loma Baya case. Ore Geology Reviews 81, 1053-1065.

Grant, T.B., Harlov, D.E., Rhede, D., 2016. Experimental formation of pyroxenites veins by reactions between olivine and Si, Al, Ca, Na, and Cl-rich fluids at 800 °C and 800 MPa: implications for fluid metasomatism in the mantle wedge. Americal Mineralogist 101 (4), 808–818. http://dx.doi.org/10.2138/am-2016-5441.

Grieco, G., Diella, V., Chaplygina, N.L., Savalieva, G.N., 2006. Platinum group elements zoning and mineralogy of chromitites from the cumulate sequence of the Nurali massif (Southern Urals, Russia). Ore Geology Reviews 30, 257–276.

Griffin, W.L., Afonso, J.C., Belousova, E.A., Gain, S.E., Gong, X.H., González-Jiménez, J. M., Howell, D., Huang, J.X., McGowan, N., Pearson, N.J., Satsukawa, T., Shi, R., Williams, P., Xiong, Q., Yang, J.S., Zhang, M., O'Reilly, S.Y., 2016. Mantle recycling: transition zone metamorphism of Tibetan ophiolitic peridotites and its tectonic implications. J. Petrol. 57, 655–684.

Frost, D.J., 2006. The stability of hydrous mantle phases. Reviews in Mineralogy and Geochemistry 62, 243-271.

Hicky, R.L., Frey, F.A., 1982. Geochemical characteristics of boninite serives volcanic: implication for their source. Geochimica et Cosmochimica Acta 46, 2099–2115.

Ishii, T., Kojitani, H., TsukamoTo, S., Fujino, K.,Mori, D., Inaguma, Y., Tsujino, N., Yoshino, T., Yamazaki, D., Higo, Y., Funakoshi, K., Akaogi, M., 2014. High-pressure phase transitions in $FeCr_2O_4$ and structure analysis of new post-spinel $FeCr_2O_4$ and $Fe_2Cr_2O_5$ phases with meteoritical and petrological implications. American Mineralogist 99, 1788–1797.

Ishii, T., Kojitani, H., Fujino, K., Yusa, H., Mori, D., Inaguma, Y., Matsushita, Y., Yamaura, K., Akaogi,M., 2015. High-pressure high-temperature transitions in$MgCr_2O_4$ and crystal structures of new $Mg_2Cr_2O_5$ and post-spinel $MgCr_2O_4$ phases with implications for ultrahigh-pressure chromitites in ophiolites. American Mineralogist 100, 59–65.

Jayananda, M., Kano, T., Peucat, J.J., Channabasappa, S., 2008. 3.35Ga komatiite volcanism in the western Dharwar craton, southern India: constraints from Nd isotopes and whole rock geochemistry, Precambrian Research 162,160-179.

Jiang, P., Kroner, A., Windley, B.F., Shi, Y., Zhang, W., Yang, W., 2012. Carboniferous and Cretaceous mafic-ultramafic massifs in Inner Mongolia (China): a SHRIMP zircon and geochemical study of the previously presumed integral "Hegenshan ophiolite". Lithos 142-143, 48-66.

Kamenetsky, V.S., Crawford, A.J., Meffre, S., 2001. Factors controlling chemistry of magmatic spinel: an empirical study of associated olivine, Cr-spinel and melt inclusions from primitive rocks. Journal of Petrology 42, 655–671.

Kimbrough, D. L., and Moore, T. E., 2003, Ophiolite and volcanic arc assemblages on the Peninsula and Cedros Island, Baja California Sur, Mexico: Mesozoic forearc lithosphere of the Cordilleran magmatic arc, in Johnson, S.E., Paterson, S.R., Fletcher, J.M., Girty, G.H., Kimbrough, D.L., and Martin-Barajas, A., eds., Tectonic evolution of northwestern Mexico and the southwestern USA: GSA Special Paper 374, p. 43–71.

Marchesi, C., Garrido, C.J., Bosch, D., Bodinier, J.-L., Hidas, K., Padrón-Navarta, J.A., Gervilla, F., 2012. A Late Oligocene Suprasubduction Setting in the Westernmost Mediterranean Revealed by Intrusive Pyroxenite Dikes in the Ronda Peridotite (Southern Spain). Journal of Geology 120, 237-247.

Marocchi, M., Hermann, J., Tropper, P., Bargossi, G.M., Mair, V., 2010. Amphibole and phlogopite in "hybrid" metasomatic bands monitor trace element transfer at the slab–mantle interface (eastern Alps, Italy). Lithos 117,135–148.

Matveev, S., Ballhaus, C., 2002. Role of water in the origin of podiform chromitite deposits. Earth and Planetary Science Letters 203, 235–243.

McGowan, N.M., Griffin, W.L., González-Jiménez, J.M., Belousova, E., Afonso, J.C., Shi, R., McCammon, C.A., Pearson, N.J., O'Reilly, S.Y., 2015. Tibetan chromitites: excavating the slab graveyard. Geology 43 (2), 179-182.

Melcher, F., Grum, W., Simon, G., Thalhammer, T.V., Stumpfl, E.F., 1997. Petrogenesis of the ophiolitic giant chromite deposits of Kempirsai, Kazakhstan: a study of solid and fluid inclusions in chromite. Journal of Petrology 38, 1419–1458.

Miura, M., Arai, S., Ahmed, A.H., Mizukami, M., Okuno, M., Yamamoto, S., 2012. Podiform chromitite classification revisited: a comparison of discordant and concordant chromitite pods fromWadi Hilti, northern Oman ophiolite. Journal of Asian Earth Sciences 59, 52–61.

Mondal, S.K., Ripley, E.M., Li, C., Frei, R., 2006. The genesis of Archean chromitites from the Nuasahi and Sukinda massifs in the Singhbhum craton, India. Precambrian Research 148, 45–66.

Naldrett, A.J., Duke, J.M., 1980. Pt metals in magmatic sulphide ores. Sciences 208, 1417–1424.

Naldrett, A.J., Wilson, A., Kinnaird, J., Yudovskaya, M., Chunnett, G., 2011. The origin of chromitites and related PGE mineraliszation in the Bushveld Complex: new mineralogical and petrological constraints. Mineralium Deposita. http://dx.doi.org/10.1007/ s00126-011-0366-3.

O'Driscoll, B., González-Jiménez, J.M., 2016. Petrogenesis of the Platinum-group minerals. Reviews in Mineralogy and Geochemistry 81, 489-578.

Ortega-Obregón, C., Solari, L., Gómez-Tuena, A., Elías-Herrera, M., Ortega-Gutiérrez, F., Macías-Romo, C., 2014. Permian–Carboniferous arc magmatism in southern Mexico: U–Pb dating, trace element and Hf isotopic evidence on zircons of ear-liest subduction beneath the western margin of Gondwana. Internationa Journal of Earth Sciencies (Geologische Rundschau) 103, 1287–1300.

Pagé, P., Barnes, S.J., 2009. Using trace elements in chromite to constrain the origin of podiform chromitites in the Thetfod Mines ophiolite, Québec, Canada. Economic Geology 104, 997–1018.

Pearson, D.G., Parman, S.W., Nowell, G.M., 2007. A link between large mantle melting events and continent growth seen in osmium isotopes. Nature 449, 202–205.

Petrou, A. and Economou-Eliopoulos, M., 2009. The activation energy values estimated by the Arrhenius equation as a controlling factor of platinum-group mineral formation. Geochimica et Cosmochimica Acta 73, 1625-1636.

Prencipe, M., Mantovani, L., Tribaudino, M., Bersani, D., Lottici, P.P. (2012). The Raman spectrum of diopside: a comparison between ab initio calculated and experimentally measured frequencies. European Journal of Mineralogy, 24, 457-464.

Prichard, H.M., Neary, C.R., Fisher, F.C., O'Hara, M.J., 2008. PGE-rich Podiform chromitites in the Al'Ays ophiolite complex, Saudi Arabia: an example of critical mantle melting to extract and concentrate PGE. Economic Geology 103, 1507–1529.

Proenza, J.A., Gervilla, F., Melgarejo, J.C., Bodinier, J.L., 1999. Al- and Cr-rich chromitites from the Mayarí-Baracoa Ophiolitic Belt (Eastern Cuba): consequence of interaction between volatile-rich melts and peridotites in suprasubduction mantle. Economic Geology 94, 547–566.

Proenza, J., Zaccarini, F., Lewis, J., Longo, F., Garuti, G., 2007. Chromian spinel composition and the platinum-group minerals of the PGE-rich Loma Peguera chromitites, Loma Caribe peridotites, Dominican Republic. The Canadian Mineralogist 45, 631–648.

Prouteau, G., Scaillet, B., Pichavant, M., Maury, R., 2001. Evidence for mantle metasomatism by hydrous silicic melts derived from subducted oceanic crust. Nature 410, 197–200.

Radelli, L., 2008. Ultrabasic-basic intrusive Layered Complex and Ophiolite (southern Baja California, Mexico). Boletín de Geología 30,1, 77-97.

Robinson, P. T., Trumbull, R. B., Schmitt, Z., Yang, J.-S., Li, J.-W., Zhou, M.-F., Erzinger, J., Dare, S., Xiong, F., 2015. The origin and significance of crustal minerals in ophiolitic chromitites and peridotites. Gondwana Research 27, 486–506.

Rojas-Agramonte, Y., García-Casco, A., Kemp, A., Kröner, A., Proenza, J.A., Lázaro, C., Liu, D., 2016. Recycling and transport of continental material through the mantle wedge above subduction zones: A Caribbean example. Earth and Planetary Science Letters, in press.

Rollison, H., 2008. The geochemistry of mantle chromitites from the northern part of the Oman ophiolite: inferred parental melt compositions. Contributions to Mineralogy and Petrology 156, 273-288.

Rollinson, H., 2016. Surprises from the top of the mantle transition zone. Geology Today 32, 2, 58-64.

Ruskov, T., Spirov, I., Georgieva, M., Yamamoto, S., Green, H.W., McCammon, C.A., Dobrzhinetskaya, L.F., 2010. Mossbauer spectroscopy studies of the valence state of iron in chromite from the Luobusa massif of Tibet: implications for a highly reduced deep mantle. Journal of Metamosphic Geology 28, 551–560.

Satsukawa, T., Griffin, W. L., Piazolo, S.,O'Reilly, S.Y., 2015. Messengers from the deep: Fossil wadsleyite–chromite microstructures from the Mantle Transition Zone. Scientific Reports 5, 16484, doi:10.1038/srep16484.

Scholl, D. W., and von Huene, R., 2007. Crustal recycling at modern subduction zones applied to the past: Issues of growth and preservation of continental basement crust, mantle geochemistry, and supercontinent reconstruction, Mem. Geol. Soc. Am., 200, 9–32.

Scholl, D.W., von Huene, R., 2009. Implications of estimated magmatic additions and recycling losses at the subduction zones of accretionary (non-collisional) and collisional (suturing) orogens. Geol. Soc. (Lond.) Spec. Publ.318, 105–125.

Sedlock, R.L., Ortega-Gutiérrez, F., and Speed, R.C., 1993. Tectonostratigraphic terranes and tectonic evolution of Mexico, Geological Society of America Special Paper 278, 153pp.

Shaw, S.E., Todd, V.R., Kimbrough, D.L., Pearson, N.J., 2014, A west-to-east geologic transect across the Peninsular Ranges batholith, San Diego County, California: Zircon 176 Hf/177 Hf evidence for the mixing of crustal- and mantle derived magmas, and comparisons with the Sierra Nevada batholith, in Morton, D.M., and Miller, F.K., eds. , Peninsular Ranges Batholith, Baja California and Southern California: Geological Society of America Memoirs, v. 211, p. 499–536, http://dx.doi.org/10.1130/2014.1211(15).

Sizova, E., Gerya,T., Brown, M., Perchuk, L.L., 2009. Subduction styles in the Precambrian: Insight from numerical experiments. Lithos, doi:10.1016/j.lithos.2009.05.028.

Solari, L.A., Dostal, J., Ortega-Gutiérrez, F., Keppie, D.J., 2001. The 275 Ma arc-related La Carbonera stock in the northern Oaxacan Complex of southern Mexico: U-Pb geochronology and geochemistry. Revista Mexicana de Ciencias Geológicas 18, 2, 149-161.

Talavera-Mendoza, O., Ruiz, J., Gehrels, G. E., Meza-Figueroa, D. M., Vega-Granillo, R., Campa-Uranga, M. F., 2005. U–Pb geochronology of the Acatlán Complex and implications for the Paleozoic paleogeography and tectonic evolution of southern Mexico. Earth and Planetary Science Letters 235, 682-699.

Tarkian, M., Nadienova, E., Zhelyaskova-Panayotova, M., 1991. Platinum-group minerals in chromitites from the eastern Rhodope ultramafic complex, Bulgaria. Mineralogy and Petrology 44, 73–87.

Ulmer, P., Trommsdorff, V., 1999. Phase relations of hydrous mantle subducted to 300 km. In Mantle Petrology: Field Observations and High-pressure Experimentation. Fei Y, Bertka CM, Mysen BO (ed) Geochemical Society, Special Publication 6, 259-281.

Uysal, I., Tarkian, M., Sadiklar, M.B., Zaccarini, F., Meisel, T., Garuti, G., Heidrich, S., 2009. Petrology of high-Cr and high-Al ophiolitic chromitites from the Muğla, SW Turkey: implications from composition of chromite, solid inclusions of platinum-group mineral (PGM), silicate, and base-metal mineral (BMM), and Os-isotope geochemistry. Contributions to Mineralogy and Petrology 158, 659–674.

Valley, J.W., Lackey, J.S., Cavosie, A.J., Clechenko, C.C., Spicuzza, M.J., Basei, M.A.S., Bindeman, I.N., Ferreira, V.P., Sial, A.N., King, E.M., Peck, W.H., Sinha, A.K., Wei, C. S., 2005. 4.4 billion years of crustal maturation: oxygen isotopes in magmatic zircon. Contributions to Mineralogy and Petrology 150, 561–580. http://dx.doi.org/10.1007/s00410-005-0025-8.

Vatin-Perignon, N., Amossé, J., Radelli, L., Keller, F., Castro-Leyva, T., 2000. Platinum group element behaviour and thermochemical constraints in the ultrabasic–basic complex of the Peninsula, Baja California Sur, Mexico. Lithos 53, 59–80.

Wilson, M., 1989. Igneous Petrogenesis. London: Unwin Hyman.

Wu, Y., Xu., M., Jin, Z., Fei., Y., Robinson, P.T., 2016. Experimental constraints on the formation of the Tibetan podiform chromitites. Lithos 245, 109-117.

Xiong, F., Yang, J., Robinson, P.T., Xu, X., Liu, Z., Li, Y., Li, J., Chen, S., 2015. Origin of podiform chromitite, a new model based on the Luobusa ophiolite, Tibet. Gondwana Research 27, 525–542.

Xiong, Q., Henry, H., Griffin, W.L., Zheng, J.P., Satsukawa, T., Pearson, N.J., O'Reilly, S.Y., 2017. High- and low- Cr chromitite and dunite in a Tibetan ophiolite: evolution from mature subduction system to incipient forearc in the Neo- Tethyan Ocean. Contributions to Mineralogy and Petrology 172, 45. DOI 10.1007/s00410-017-1364-y.

Xu, X., Yang, J., Robinson, P., Xiong, F., Ba, D., Guo, G., 2015. Origin of ultrahigh pressure and highly reduced minerals in podiform chromitites and associated peridotites of the Luobusa ophiolite. Tibet. Gondwana Research 27, 686–700.

Yamamoto, S., Komiya, T., Hirose, K., Maruyama, S., 2009. Coesite and clinopyorexene exsolution lamellae in chromite: in-situ ultrahigh-pressure evidence from podiform chromitites in the Luobusa ophiolite, southern Tibet. Earth and Planetary Science Letters 109, 314–322.

Yamamoto, S., Komiya, T., Yamamoto, H., Kaneko, Y., Terabayashi, M., Katayama, I., Iizuka, T., Maruyama, S., Yang, J., Kon, Y., Hirata, T., 2013. Recycled crustal zircons from podiform chromitites in the Luobusa ophiolite, southern Tibet. The Island Arc 22, 89–103.

Yang, J.-S., Dobrzhinetskaya, L., Bai, W.-J., Fang, Q.-S., Robinson, P.T., Zhang, J., Green II. H.W., 2007. Diamond- and coesite-bearing chromitites from the Luobusa ophiolite Tibet. Geology 35, 875–878.

Yang, J. S., Meng,. F., Xu, S., Robinson, P. T., Dilek, Y., Makeyev, A. B., Wirth, R., Wiedenbeck, M., Cliff, J., 2015. Diamonds, native elements and metal alloys from chromitite of the Ray-Iz ophiolite of the Polar Urals. Gondwana Research 27, 459–485.

Zaccarini, F., Pushkarev, E.V., Fershtater, B., Garuti, G., 2004. Composition and mineralogy of PGE-rich chromitites in the Nurali lherzolite–gabbro complex, southern Urals, Russia. The Canadian Mineralogist 42, 545–562.

Zandt, G., Gilbert, H., Owens, T.J., Ducea, M., Saleeby, J., Jones, C.H., 2004. Active foundering of a continental arc root beneath the southern Sierra Nevada in California. Nature 431, 41–46.

Zanetti, A., Giovanardi, T., Langone, A., Tiepolo, M., Wu, F-Y., Dallai, L., Mazzucchelli., M., 2016. Origin and age of zircon-bearing chromitite layers from the Finero phlogopite peridotite (Ivrea–Verbano Zone,Western Alps) and geodynamic consequences. Lithos 262, 58-74.

Zhang, Y., Jin, Z., Griffin, W.L., Wang, C., Wu, Y., 2017. High-pressure experiments provide insights into the Mantle Transition Zone history of chromitite in Tibetan ophiolites. Earth and Planetary Science Letters, 463, 151-158

Zhou, M.F., Robinson, P.T., Su, B.X., Gao, J.F., Li, J.W., Yang, J.S., Malpas, J., 2014. Compositions of chromite, associated minerals, and parental magmas of podiform chromite deposits: The role of slab contamination of asthenospheric melts in suprasubduction zone envrionments. Gondwana Research 26 (1), 262-283.

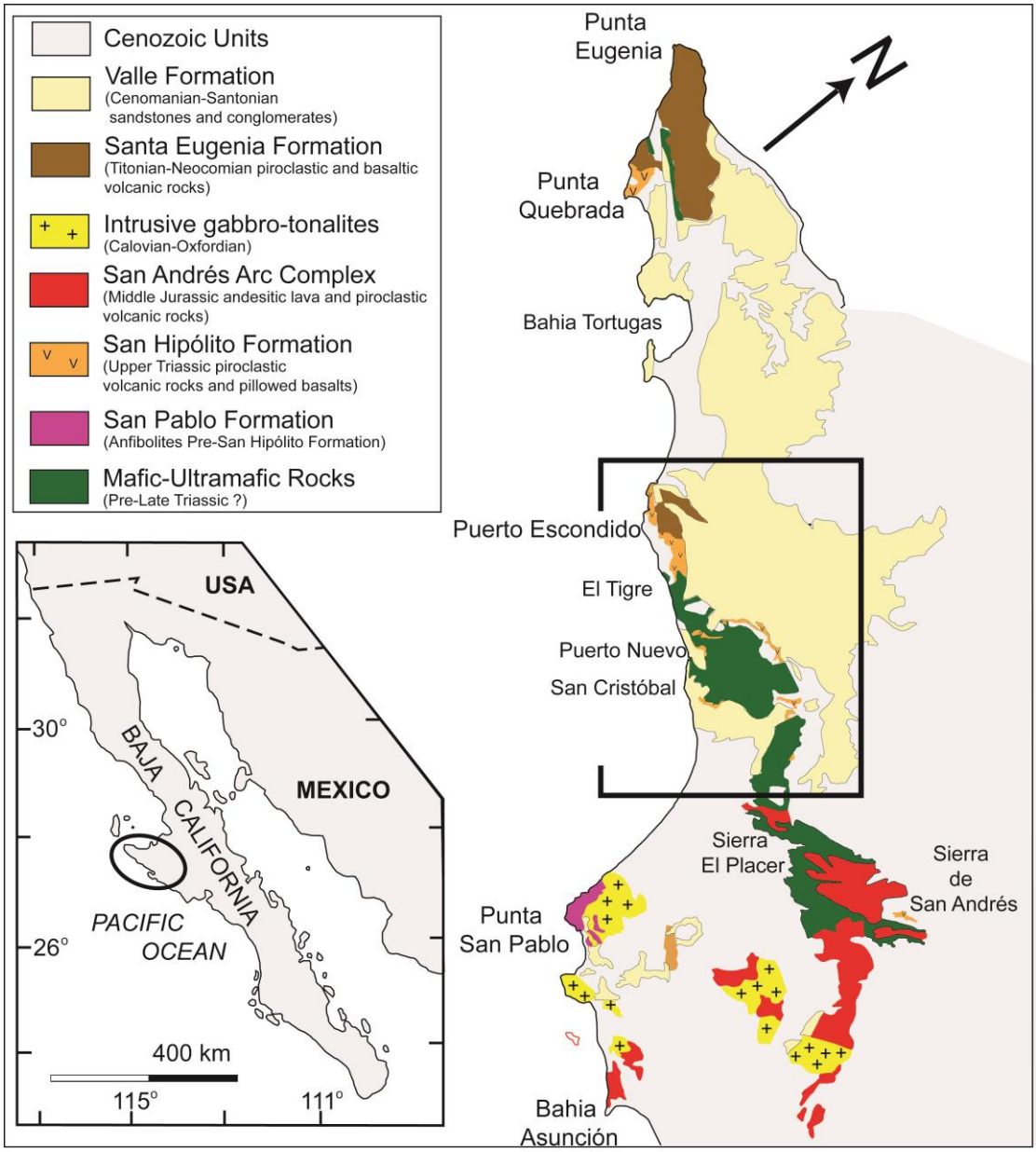

Figure 1

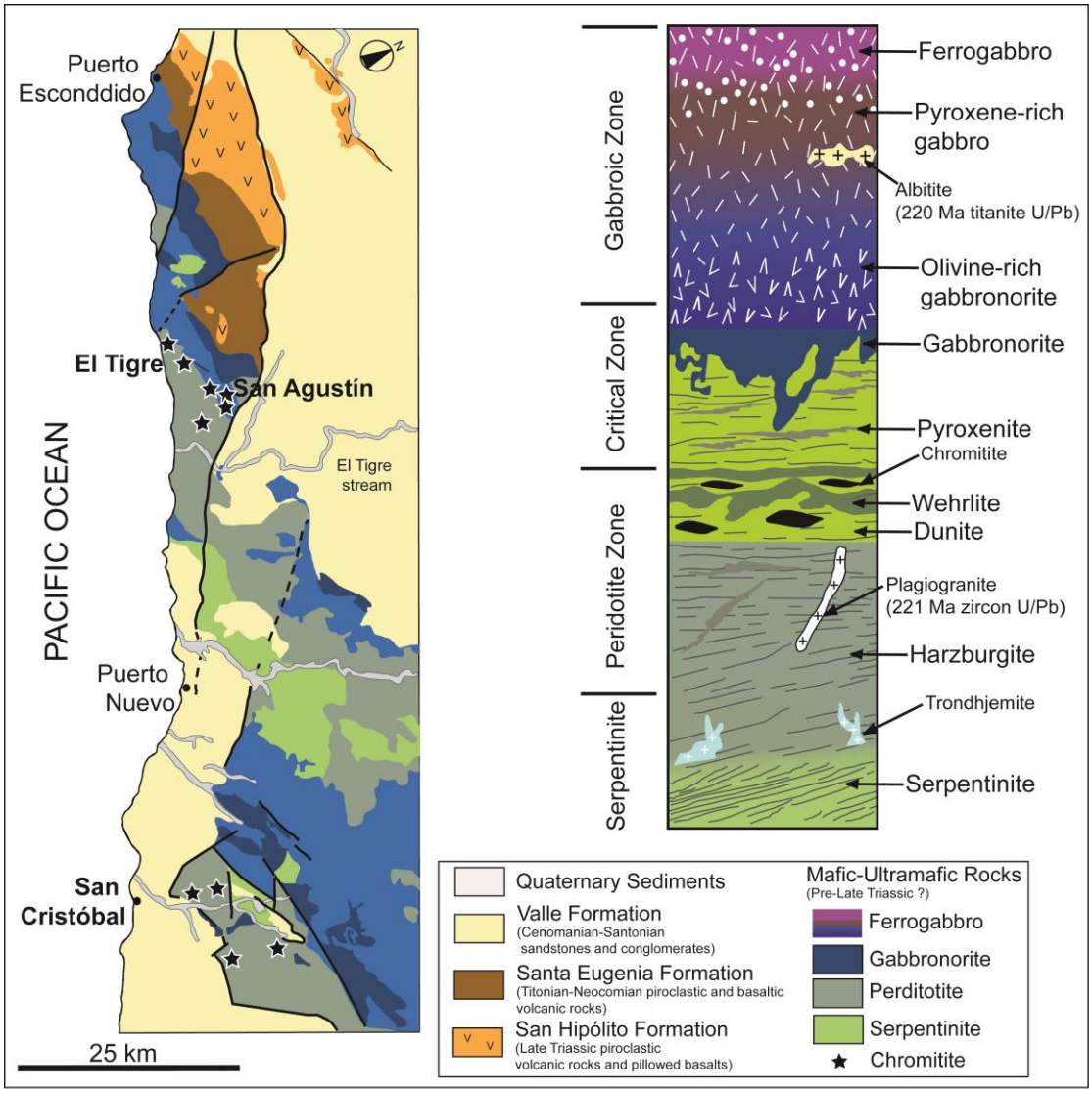

Figure 2

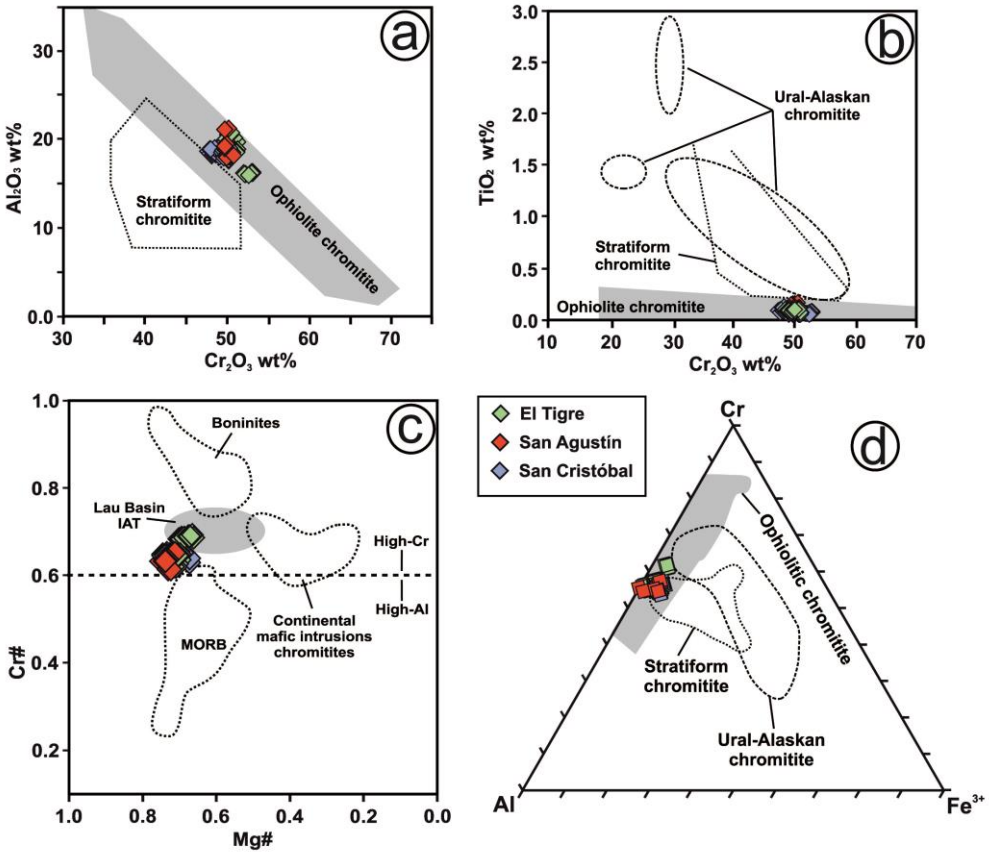

Figure 3

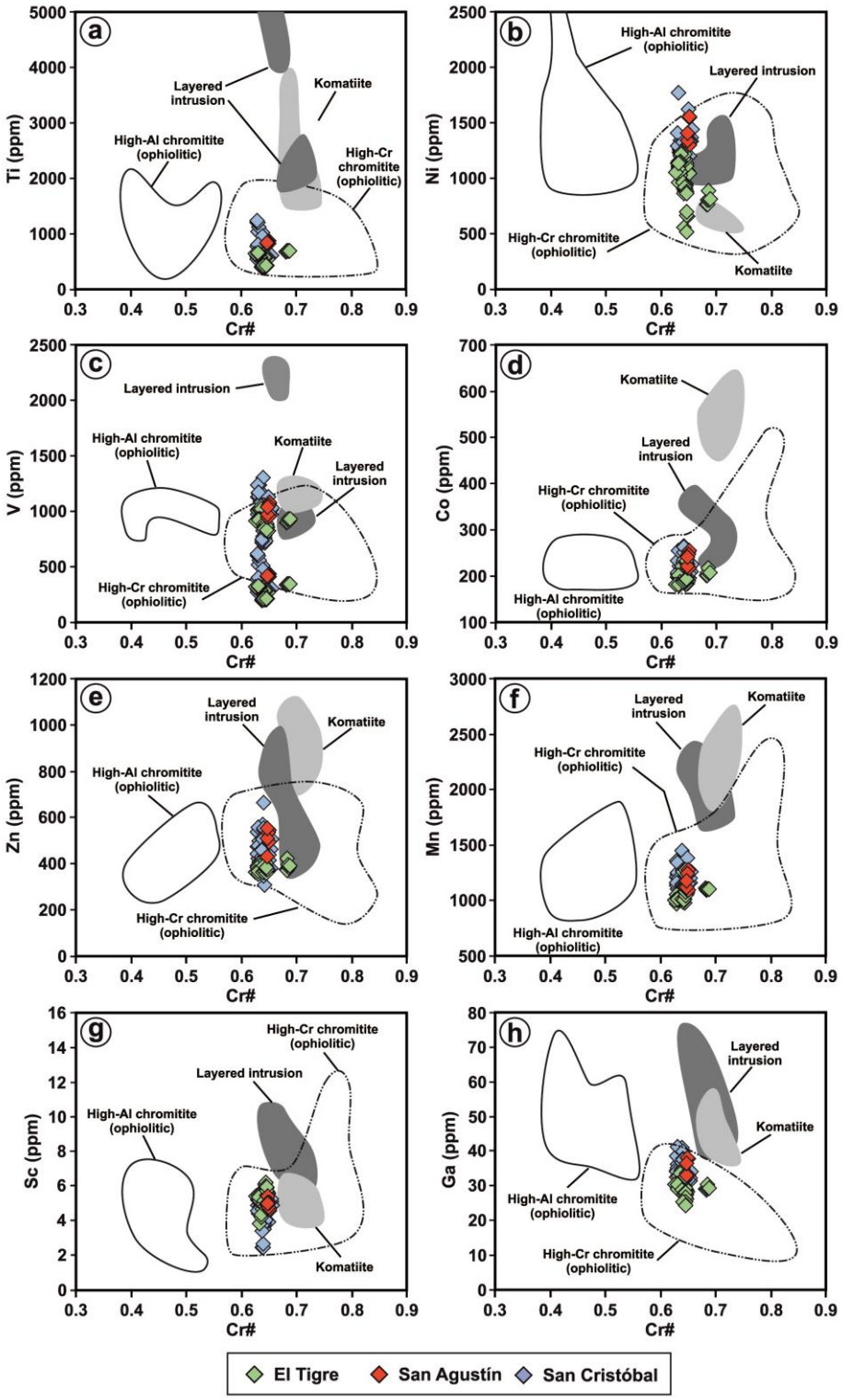

Figure 4

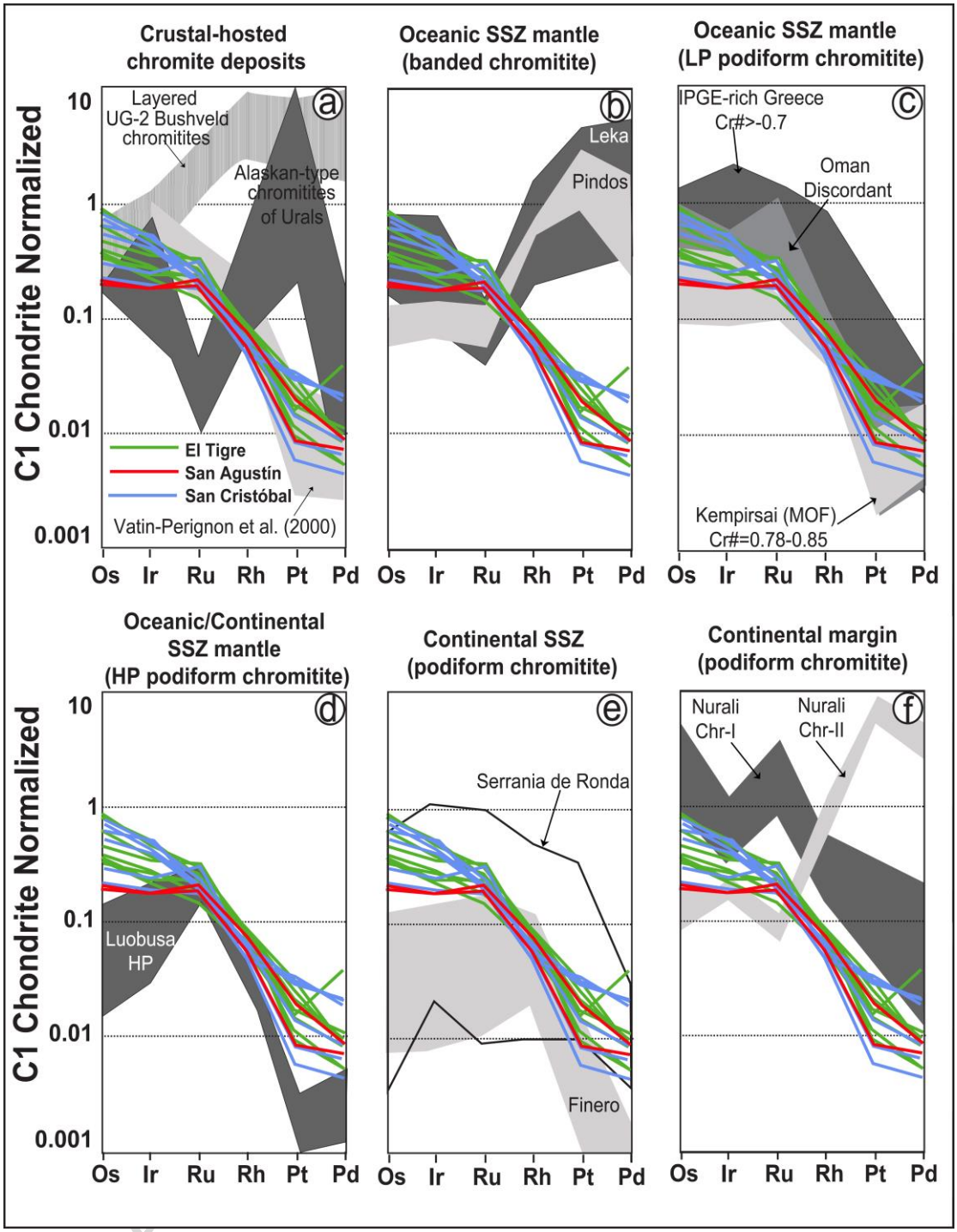

Figure 5

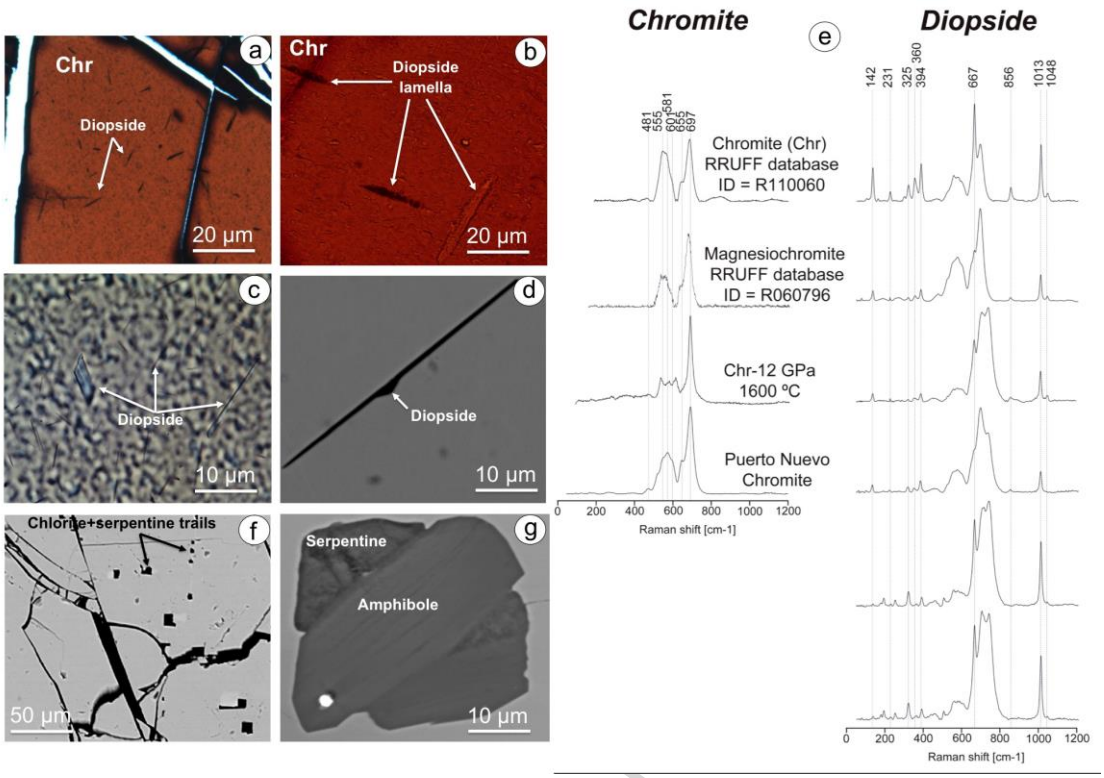

Figure 6

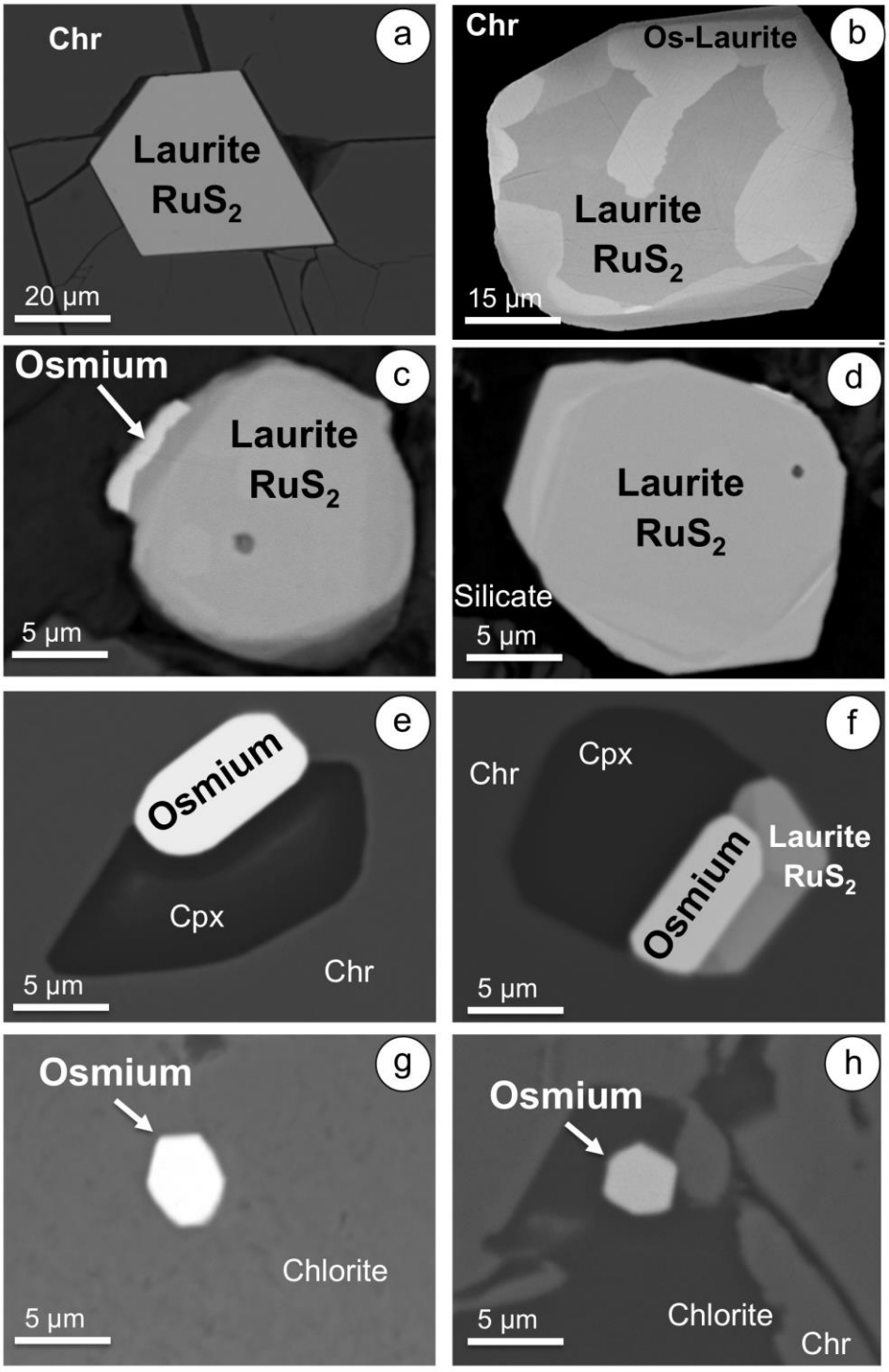

Figure 7

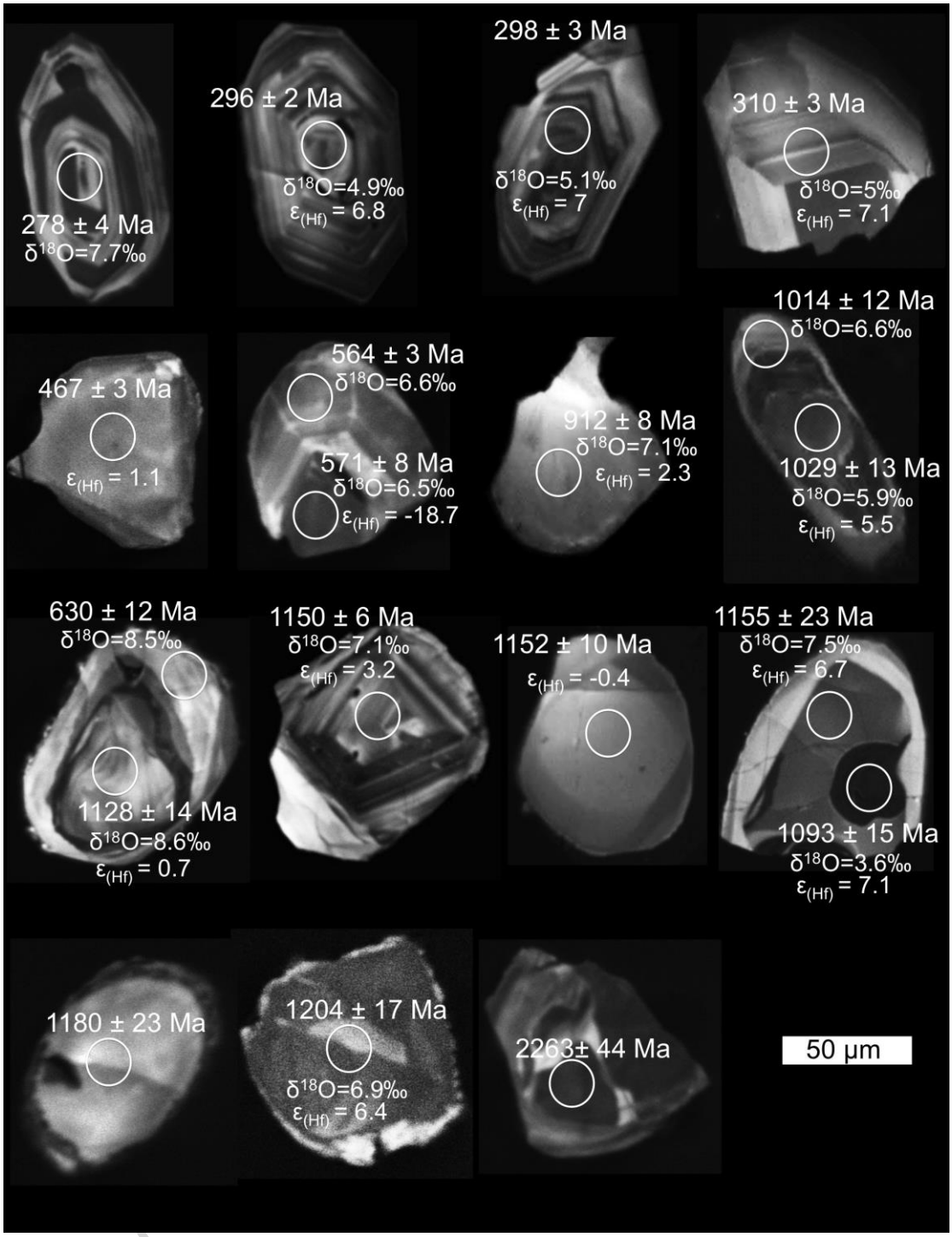

Figure 8

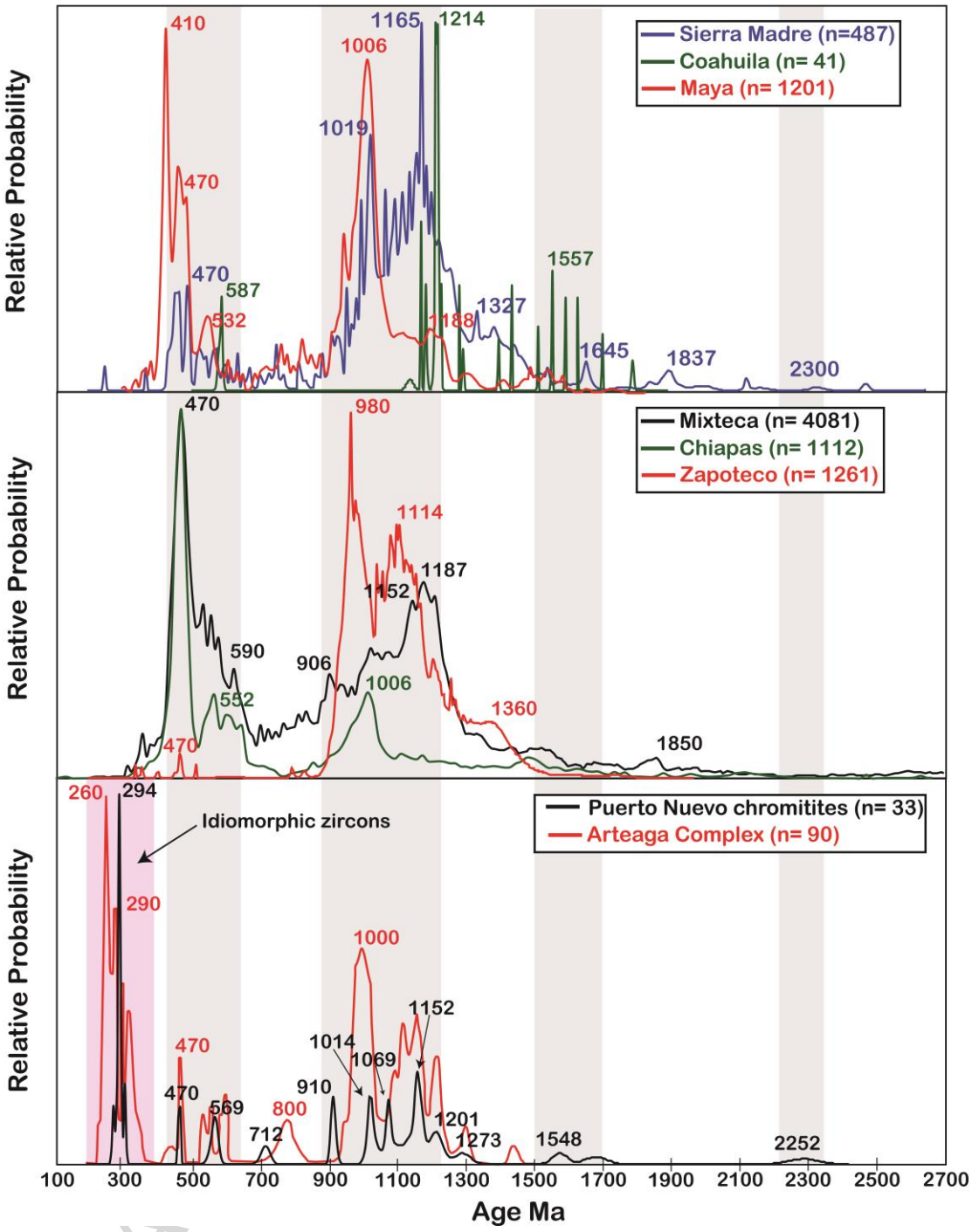

Figure 9

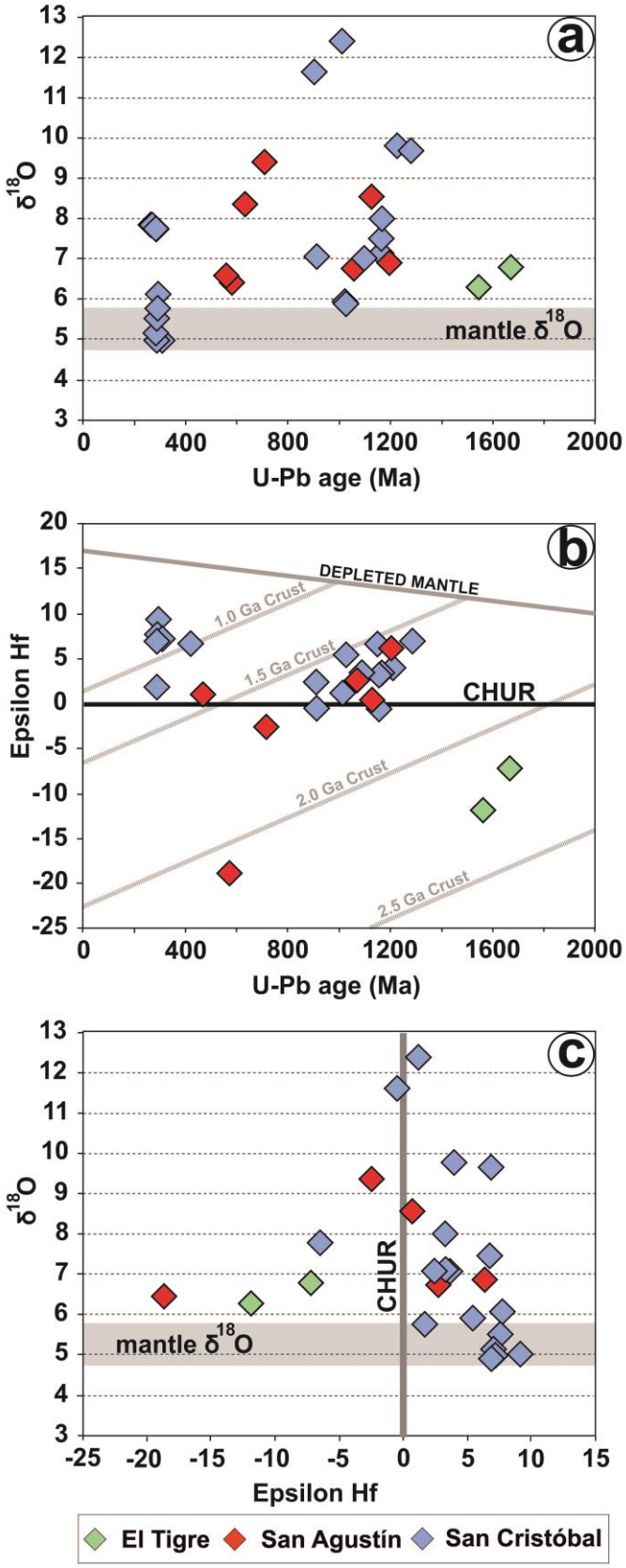

Figure 10

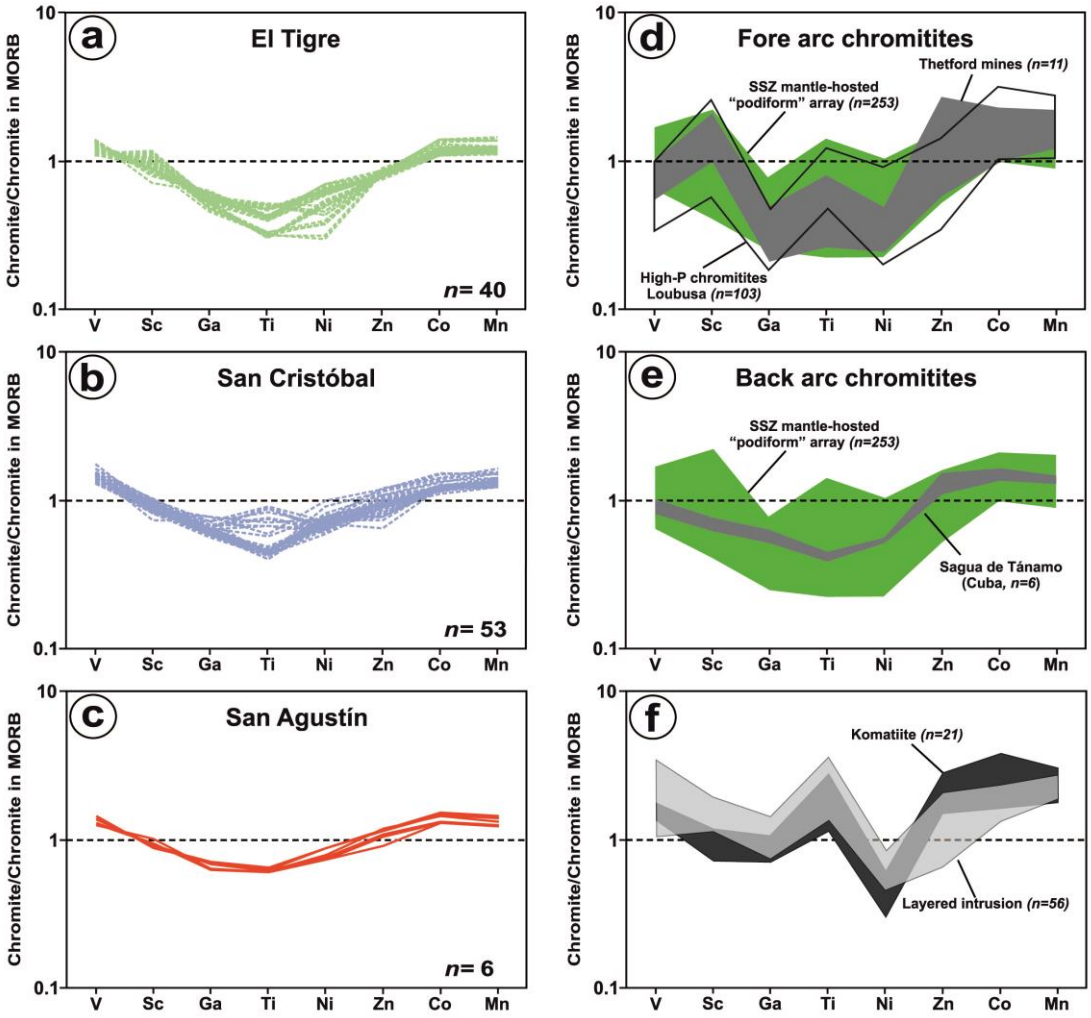

Figure 11

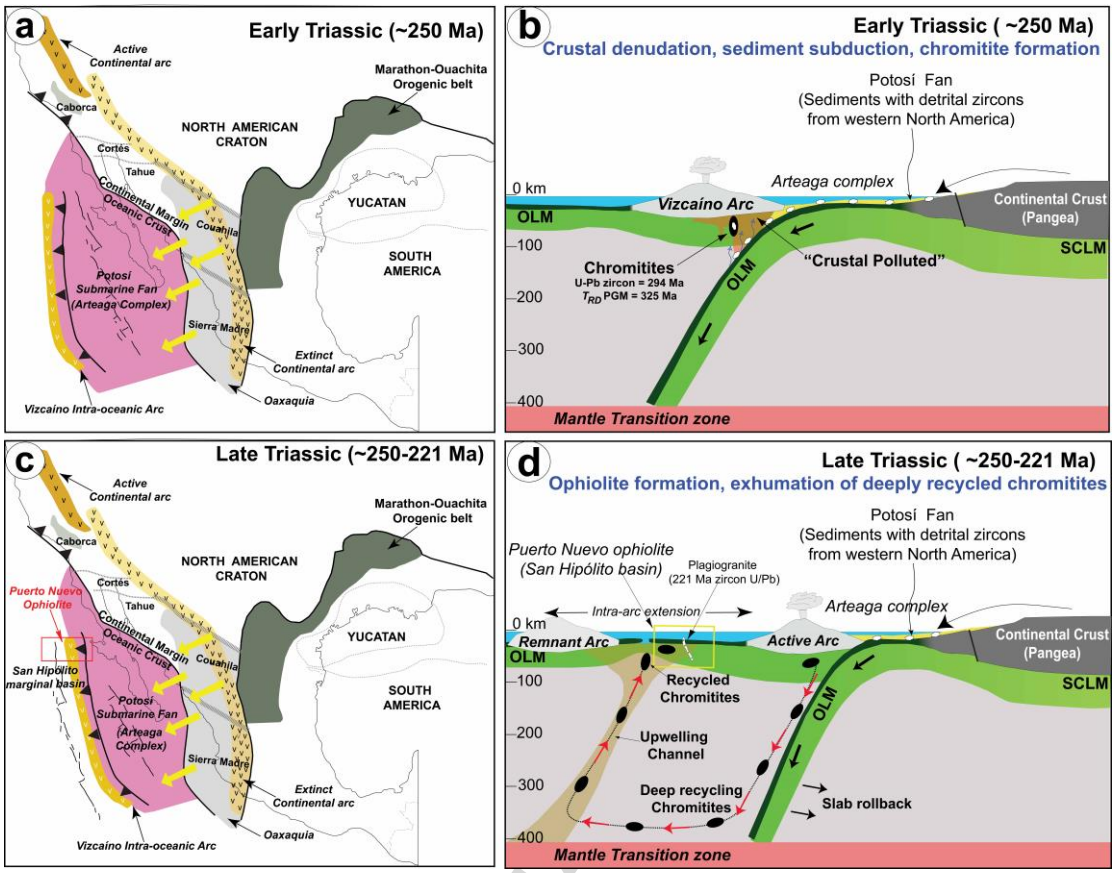

Figure 12

Table 1. Platinum-group elements of chromitite samples from Puerto Nuevo (in ppb).

	Os	Ir	Ru	Rh	Pt	Pd
SA1-100D	108	102	154	16	21	5
SA1-100F	113	102	135	12	9	4
SC1-101C	285	245	133	11	27	10
SC1-101C A	345	233	137	10	25	10
SC1-102B	245	189	111	8	30	9
SC1-102C	278	204	119	9	26	9
SC1-103B	324	200	136	10	12	4
SC2-100A	319	204	125	11	12	4
SC3-101A	127	115	185	8	7	3
SC4-100A	100	90	106	9	5	2
SC4-101D	122	126	122	11	130	3
T1-100B	204	155	129	16	23	6
T1-101C	177	126	103	13	15	5
T2-100B	450	263	217	18	27	5
T2-100D	433	285	172	18	10	3
T3-100A	235	197	214	15	12	3
T3-100B	176	150	161	17	33	5
T4-100E	332	208	184	13	18	6
T4-100G	190	129	168	14	16	21

Table 2. . Representative analyses of platinum-group from the Puerto Nuevo chromitites.

Sample/Grain	Mineral	Os	Ir	Ru	Pt	Pd	Rh	Fe	Cr	Ni	Cu	Co	S	As	Total	Os apfu	Ir apfu	Ru apfu	Pt apfu	Rh apfu	Fe apfu	Ni apfu	S apfu	As apfu
T2-100B-1-PTO1-6	Laurite	14.18	6.72	41.85	0.00	1.52	0.60	0.43	0.92	0.23	0.00	0.00	34.27	0.00	100.72	0.14	0.07	0.77	0.00	0.01	0.01	0.01	1.99	0.00
T2-100B-1-PTO1-7	Laurite	10.53	3.57	48.68	0.00	1.75	0.57	0.27	0.15	0.15	0.02	0.00	35.29	0.00	100.98	0.10	0.03	0.87	0.00	0.01	0.01	0.00	1.98	0.00
T2-100B-D-pto3-2	Laurite	12.41	6.79	43.86	0.00	0.00	1.08	0.11	0.22	0.05	0.10	0.00	34.89	0.00	99.52	0.12	0.06	0.80	0.00	0.02	0.00	0.00	2.00	0.00
T2-100B-D-pto3-3	Laurite	12.50	6.73	44.00	0.00	0.00	1.10	0.13	0.32	0.05	0.08	0.01	34.92	0.00	99.84	0.12	0.06	0.80	0.00	0.02	0.00	0.00	1.99	0.00
T2-100B-D-pto3-4	Laurite	12.42	6.69	43.98	0.00	0.00	1.10	0.15	0.39	0.04	0.08	0.00	34.92	0.00	99.77	0.12	0.06	0.80	0.00	0.02	0.00	0.00	1.99	0.00
T2-100B-D-pto3-5	Laurite	12.43	6.81	44.00	0.02	0.00	1.13	0.11	0.18	0.05	0.08	0.01	34.91	0.00	99.73	0.12	0.06	0.80	0.00	0.02	0.00	0.00	1.99	0.00
SC2-100A-F-pto2-2	Laurite	12.94	6.72	43.36	0.00	0.00	0.62	0.49	1.18	0.06	0.08	0.02	34.42	0.00	99.87	0.13	0.06	0.79	0.00	0.01	0.02	0.00	1.99	0.00
SC2-100A-F-pto2-3	Laurite	12.78	6.76	43.29	0.00	0.00	0.70	0.54	1.21	0.05	0.08	0.00	33.99	0.00	99.40	0.13	0.07	0.80	0.00	0.01	0.02	0.00	1.98	0.00
T2-100B-5-PTO6-1	Os-Laurite	23.91	4.05	37.06	0.00	1.35	0.49	0.30	0.90	0.09	0.00	0.00	32.57	0.22	100.94	0.24	0.04	0.71	0.00	0.01	0.01	0.00	1.97	0.01
T2-100B-5-PTO6-2	Os-Laurite	28.15	3.80	32.91	0.00	1.24	0.38	0.31	0.87	0.09	0.02	0.00	31.23	0.18	99.18	0.30	0.04	0.66	0.00	0.01	0.01	0.00	1.97	0.00
T2-100D-F-PTO1-2	Erlichmanite	56.06	12.77	0.14	0.00	0.04	4.16	0.39	0.90	0.10	0.17	0.01	25.05	0.00	99.79	0.74	0.17	0.00	0.00	0.10	0.02	0.00	1.96	0.00
T2-100B-6-PTO6-1	Osmium	60.06	32.16	4.73	0.48	0.15	0.24	0.69	2.25	0.03	0.01	0.00	0.00	0.00	100.80	0.60	0.32	0.09	1.00	0.00	0.00	0.00	0.00	0.00
T2-100B-5-PTO5-1	Irarsite	1.92	59.00	0.00	0.00	0.09	0.58	0.65	1.66	0.10	0.03	0.00	12.17	22.23	98.43	0.03	0.92	0.00	0.00	0.02	0.00	0.00	1.14	0.89

Table 3. Calculation of Al_2O_3 and TiO_2 contents and FeO/MgO ratios (wt.%) of the melts in equilibrium with chromite from Puerto Nuevo and other mantled-derived "podiform" high-Cr chromitites. The values for boninites, MORB, komatiites and layered intrusions are also presented for comparison. Ti values in the melt have been computed using the values obtained from the EMPA analysis. Details of computations are given in the Appendix 3. References: (a) Pagé and Barnes (2009); (b) Zhou et al. (2014); (c) González-Jiménez et al. (2011); (d) Proenza et al. (1999); (e) Rollinson (2008); (f) Melcher et al. (1997); (g) Ghosh et al. (2009); (h) Uysal et al. (2009); (i) Akmaz et al. (2014); (j) Uysal et al. (2016); (k) Akbulut et al. (2016); (l) Acvi et al. (2017); (m) Augé (1987); (n) Hicky and Frey (1982); (o) Wilson (1989); (p) Jayananda et al. (2008); (q) Fan and Kerrich (1997); (r) Mondal et al. (2006 and references therein).

	Al_2O_3 liquid	TiO_2 liquid	FeO/MgO liquid
	(wt.%)	(wt.%)	(wt.%)
Fore arc podiform chromitites			
Thetford Mines, Canada [(a)]	9.3-13.0	0.12-0.3	
Lobousa, Tibet [(b)]	13.8	0.31	0.97
Back arc podiform chromitites			
Sagua de Tánamo, Cuba [(c, d)]	12.91-14.15	0.22-0.39	0.9-1.5
Arc-related podiform chromitites			
Omán [(e)]	11.8-12.9	0.23-0.34	
Suprasubduction zone podiform chromitites			
Mayarí-Cristal Massif, Cuba [(d)]	11.9		0.74
Kempirsai, Kazakhstan [(f)]	9-10.6		0.3-0.5
Rutland Island, Andaman [(g)]	10.0-11.0		0.67-1.78
Muğla, Turkey [(h)]	8.8-10.5		0.3-1.1
Afşin, Turkey [(i)]	10.2-11.9	0.17-0.39	
Antalya-Isparta ophiolite, Turkey [(j)]	9.3-13.2	0.17-0.30	0.66-1.61
Lycian and Antalya, Turkey [(k)]	8.8-14.5	0.10-0.44	
Pozanti-Karsanti, Turkey [(l)]	10.7-13.7	0.19-0.44	
High-Mg IAT [(m)]	11.4–16.4		0·62±0·02
Boninitite [(n)]	10.6-14.4	0.1-0.5	0.7-1.4
MORB [(o)]	15-16	1.2-1.6	
Komatiitic basalts			
Western Dharwar Craton, India [(p)]	7.9-8.91	0.66	0.40-0.46
Abitibi greenstone belt, Canada [(q)]	8.58-9.38	0.74-0.85	0.53-0.57
Archean Layered Intrusion			
Stillwater, USA [(r)]	12.3-12.6	1.48-1.58	
Layered Intrusion			
Bushveld, South African [(r)]	11.5	0.74	
Great Dyke, Zimbabwe [(r)]	11.1	0.61	

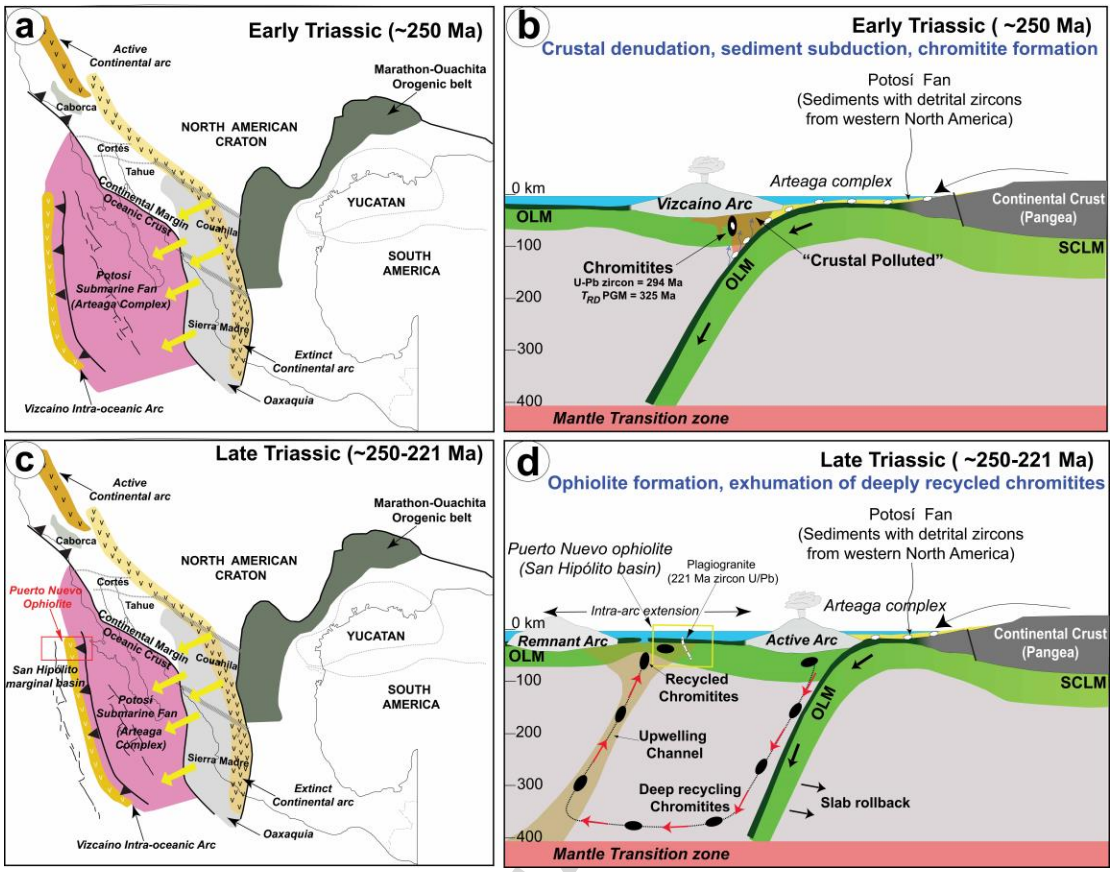

Graphical abstract

Highliths

Chromitites occur in ultramafic rocks of the Puerto Nuevo Ophiolite in the Mexican Baja California.

They are uncommon example of chromitites with low- and high-pressure assemblages

The chromitite contain crustal zircons, PGMS and pyroxene lamellae in chromite.

Formation and deep mantle recycling of chromitite is related to the evolution of intra-oceanic arc.